Blocking ActRIIB signaling and restoring appetite reverses cachexia and improves survival in mice with lung cancer

Andre Lima Queiroz
Weill Cornell Medicine
Shakti Ramsamooj
Weill Cornell Medicine
Ezequiel Dantas
Weill Cornell Medicine
Elizabeth Zunica
Pennington Biomedical Research Center
Roger Liang
Weill Cornell Medicine
Anirudh Murthy
Weill Cornell Medicine
Charles Murphy
Weill Cornell Medicine
Corey Holman
University of Pennsylvania
Curtis Bare
Weill Cornell Medicine
Gregory Ghahramani
Weill Cornell Medicine
Zhidan Wu
Pfizer Global R&D
David Cohen
Weill Cornell Medical College https://orcid.org/0000-0001-9827-6926
John Kirwan
Cleveland Clinic
Lewis Cantley
Weill Cornell Medicine https://orcid.org/0000-0002-1298-7653
Christopher Axelrod
Pennington Biomedical Research Center https://orcid.org/0000-0002-1444-8557
Marcus Goncalves (mdg9010@med.cornell.edu)

Weill Cornell Medicine https://orcid.org/0000-0002-0784-9248

Article

Keywords: Cancer, Cachexia, Energy Expenditure, Anorexia, Skeletal Muscle, Calorie Restriction

Posted Date: May 28th, 2021

DOI: https://doi.org/10.21203/rs.3.rs-563743/v1

Version of Record: A version of this preprint was published at Nature Communications on August 8th, 2022. See the published version at https://doi.org/10.1038/s41467-022-32135-0.

Blocking ActRIIB signaling and restoring appetite reverses cachexia and improves survival in mice with lung cancer

Andre Lima Queiroz[1,2], Shakti Ramsamooj[1,2], Ezequiel Dantas[1,2], Elizabeth R.M. Zunica[3], Roger J. Liang[1,2], Anirudh Murthy[1,2], Charles J Murphy[2,4,5], Corey D. Holman[6], Curtis J. Bare[6], Gregory Ghahramani[7], Zhidan Wu[8], David E. Cohen[6], John P. Kirwan[3], Lewis C. Cantley[2], Christopher L. Axelrod[3], and Marcus D. Goncalves[1,2]*

[1] Division of Endocrinology, Department of Medicine, Weill Cornell Medicine, New York, NY 10065, USA.

[2] Meyer Cancer Center, Weill Cornell Medicine, New York, NY 10065, USA

[3] Pennington Biomedical Research Center, Baton Rouge, LA, 70808, USA

[4]Center for Molecular Oncology, Memorial Sloan Kettering Cancer Center, New York, NY 10065, USA

[5] Department of Pathology, Memorial Sloan Kettering Cancer Center, New York, NY 10065, USA

[6] Division of Gastroenterology and Hepatology, Department of Medicine, Weill Cornell Medicine, New York, NY 10065, USA

[7] Weill Cornell Graduate School of Medical Sciences, Weill Cornell Medicine, New York, NY 10065, USA

[8] Internal Medicine Research Unit, Pfizer Global R&D, Cambridge, MA, USA

*Corresponding Author

Marcus D. Goncalves, MD, PhD

Assistant Professor of Medicine

Weill Cornell Medicine

413 E. 69th Street, Rm. 620

New York, NY 10021

mdg9010@med.cornell.edu

Keywords: Cancer, Cachexia, Energy Expenditure, Anorexia, Skeletal Muscle, Calorie Restriction

Abstract

The cancer anorexia-cachexia syndrome (CACS) is a common, debilitating condition with limited therapeutic options. The defining feature of CACS is weight loss, which suggests a state of negative energy balance. It is unclear whether this net reduction in energy is due solely to anorexia or if a combination of anorexia and increased energy expenditure (EE) occurs. To address this question, we induced lung cancer in mice and measured changes in food intake, EE, and body composition. Mice with CACS developed reductions in food intake, spontaneous activity, and EE. There was severe atrophy and markers of metabolic dysfunction in the adipose and skeletal muscle tissues as compared to mice without CACS and pair-fed wild-type mice. We used anamorelin fumarate (Ana), a ghrelin receptor agonist, alone or in combination ActRIIB-Fc, a ligand trap for TGF-β/activin family members, to reverse anorexia and skeletal muscle atrophy, respectively. Ana effectively increased food intake and the combination of drugs increased lean mass, restored spontaneous activity, and improved overall survival. These beneficial effects were limited to female mice. Our findings suggest that multimodal, gender-specific, therapies are needed to reverse CACS.

Introduction

The cancer anorexia cachexia syndrome (CACS) is a systemic metabolic disorder associated with increased mortality and poor quality of life [1]. CACS is defined by weight loss that preferentially affects tissues that store nutrients like skeletal muscle and adipose tissue. The loss of body weight suggests a state of negative energy balance, which could be the result of reduced food intake (anorexia), increased energy expenditure (EE), or a combination of both. While anorexia is frequently observed in CACS, it remains unclear whether the net reduction in energy balance is due solely to anorexia or if it is paired with an increase in EE.

Total energy expenditure (TEE) is controlled centrally with input from peripherally derived hormones like leptin, thyroid hormones, and glucocorticoids [2–4]. TEE can be divided into activity energy expenditure (AEE) and resting energy expenditure (REE) [5]. In this simplified model, REE encompasses the basal metabolic rate and the contribution of adaptive thermogenesis determined by changes in temperature and diet. It seems obvious that animals with cancer would have increased REE given the presence of highly metabolic tumor cells, however, the data supporting this assumption are mixed [6].

Cold-induced thermogenesis is a major contributor to REE and TEE in mice, especially when housed under standard conditions at 22°C. At this temperature, brown adipose tissue (BAT) is actively generating heat via mitochondrial uncoupling and futile cycles [7,8]. The same heat-producing pathways can be induced in white adipose tissue (WAT) in a

process called *browning*, which has been implicated in the pathogenesis of weight loss during CACS [9,10]

We and others have identified and characterized CACS in a genetically engineered mouse model of lung cancer driven by oncogenic activation of *Kras* and loss of *Stk11/Lkb1* (referred to as KL mice) [11,12]. In this model, the majority of mice develop weight loss, anorexia, and wasting of skeletal muscle and WAT independent of IL-6 and tumor burden. The penetrance of CACS phenotype is incomplete and this feature allows us to compare genetically identical, tumor-bearing mice with and without weight loss under controlled conditions.

In this study, we use the KL model to interrogate the changes in body composition, food intake, peripheral organ metabolism, and EE that occur following the induction of lung cancer. Surprisingly, we find that mice with CACS have severely low TEE driven by reductions in food intake and spontaneous activity. We attempted to reverse anorexia in mice with CACS using an anti-GDF-15 antibody, however there was no improvement in food intake. Next, we used anamorelin fumarate (Ana), a ghrelin receptor agonist, alone or in combination with a ligand trap for TGF-β/activin family members (ActRIIB-Fc) to reverse anorexia and preserve skeletal muscle. While Ana increased food intake and fat mass in both groups, only the combination of Ana and ActRIIB-Fc increased lean mass, restored spontaneous activity, and improved overall survival. These beneficial effects were limited to female mice. Our findings suggest that multimodal, gender-specific, therapies are needed to reverse CACS.

Results

Energy Expenditure is Reduced during CACS.

Following induction with an inhaled adenovirus carrying Cre recombinase (AdCre), a large proportion of KL mice (~70%) from each cohort develop CACS, defined as 15% body weight loss [11]. The loss of body weight is due to a reduction of both lean and fat mass that occurs concomitantly at a late stage (~7-8 weeks after induction) (Figures 1A and 1B). We previously showed that the loss of lean mass is due, in part, to atrophy of glycolytic skeletal muscle fibers [11]. The loss in total body fat mass is reflected in the mass of the gonadal white adipose tissue (gWAT) and interscapular brown adipose tissue (BAT), which both reduced linearly with the total weight loss (Figures S1A and S1B). The loss in gWAT mass was associated with dramatic atrophy of these adipocytes in mice with CACS as revealed by the H&E staining, an effect that was not observed in the BAT of these mice (Figure S1C).

Given the striking histologic alterations in the gWAT, we performed RNA-Seq using tissues from mice with and without CACS. At a whole-transcriptome level, mice with and without CACS clustered independently in an unbiased principal component analysis (Figure S1D). The WAT from mice with CACS was strongly enriched in BAT-like cells based on a transcriptome analysis (BATLAS) (Figure S1E) [13]. We confirmed this result by measuring the UCP1 protein abundance by immunostaining (Figure S1F) and mRNA expression (Figures S1H) of UCP1 and PGC1α in the gWAT. UCP1 expression was increased over 50-fold and UCP1-positive cells were found throughout the gWAT in mice with CACS but not in WT or non-CACS mice. In contrast, the expression level and staining

intensity of UCP1 was reduced in the BAT as well as the mRNA expression (Figures S1F, S1G, and S1I). Leptin, an adipokine that regulates food intake and energy expenditure, was dramatically reduced in the gWAT at the level of mRNA expression (Figure S1H) and in the serum (Figure S1J). We also observed higher rates of tissue lipolysis and an increased abundance of non-esterified fatty acids (NEFA) in the serum, suggesting the presence of lipolysis *in vivo* in mice with CACS (Figures S1K and S1L).

In order to assess the contribution of adaptive thermogenesis to CACS, we performed a prospective, randomized, controlled trial (RCT) where KL mice were induced at 22°C and then randomly assigned to stay at 22°C or move to 30°C four weeks after induction to allow for normal tumor development. This thermoneutral intervention did not alter the pattern of weight loss or improve overall survival (Figures S2C and S2D). Surprisingly, we observed that the EE of mice with CACS was much lower than mice without CACS at both temperatures (Figure 1C). Similar trends were observed for oxygen consumption (VO2) and the respiratory exchange ratio (Figures S2A and S2B). The values for total daily energy expenditure (TEE) were plotted against lean mass and compared to wild type (WT) mice (*i.e.* KL littermates that never received tumor induction) and tumor-bearing mice that did not have CACS at the time of the measurement but later developed CACS (Pre-CACS) (Figure 1D). We observed a stepwise reduction in TEE with WT values being the highest, mice with CACS (+CACS) being the lowest, and the Pre-CACS and tumor-bearing weight stable (-CACS) mice having intermediate values. No tumor-bearing mice had higher TEE than WT. Furthermore, the mice with CACS had lower food intake and spontaneous activity as compared to mice without CACS, however the effect on activity

faded when mice were housed at thermoneutrality (Figures 1E and 1F). These data show that mice with CACS have reduced TEE and food intake despite increased biomarkers of adipose browning. As we previously reported[11], there was a significant increase in corticosterone levels in mice with CACS but no changes in catecholamines, thyroid hormones, or insulin (Figure S3). Together, these results suggest that anorexia and hypometabolism contribute to a state of negative energy balance during CACS.

Mice with CACS Have Impaired Skeletal Muscle Metabolism.

There is a disproportionate reduction in TEE following weight loss from CACS, which is similar to what is observed following weight loss in obese humans [14]. In this setting, there is a decline in skeletal muscle glycolytic enzyme activity (as assessed by phosphofructokinase, PFK, activity), which increases muscle work efficiency [15] . We previously demonstrated and now confirm that the reduction in skeletal muscle mass in KL mice experiencing CACS is specific to muscles containing glycolytic, fast-twitch fibers (Figures S4A and S4B). We measured the activity of PFK in a glycolytic (EDL) and oxidative (Soleus) skeletal muscle from mice with and without CACS. As expected, PFK activity was higher in the EDL as compared to Soleus and it was lowered by CACS only in the EDL (Figure 2A). We also surveyed the activity of other metabolic enzymes using phosphorylation-based biomarkers that correlate with enzyme activity. For example, the phosphorylation of LDHA at Tyrosine 10 correlates with higher activity of the enzyme [16]. This modification was increased in the EDL but not the Soleus of mice with CACS (Figure 2B). In addition, the phosphorylation of PDHE1α at serine 293 is associated with lower enzymatic activity [17] and this biomarker was also increased specifically in the EDL of mice

with CACS (Figure 2B). These results suggest an overall reduction in pyruvate oxidation in fast-twitch muscles.

We performed RNA-seq using the gastrocnemius muscle from mice with and without CACS in order to identify transcriptional changes that could be related to changes in skeletal muscle metabolism. At a whole-transcriptome level, mice with and without CACS clustered independently in an unbiased principal component analysis (Figure S5A). A pathway enrichment analysis using the differentially expressed genes between the two groups identified multiple downregulated gene sets related to mitochondrial function (Figure S5B). In accordance with these changes in gene expression, we found that the mitochondrial DNA content and the abundance of mitochondrial proteins were reduced specifically in the EDL of mice with CACS (Figures 2C and 2D). However, other measures of mitochondrial structure and function showed no difference. For example, there were no consistent alterations at the ultrastructural level (Figure S5C), no change in whole muscle citrate synthase activity (Figure S5F), and no difference in the oxidative phosphorylation or electron transfer capacity of permeabilized soleus and EDL fibers (Figures S5D and S5E). Thyroid hormones are known to alter skeletal muscle metabolism during weight loss but there was no change in the abundance of T3 and T4 in muscle extracts (Figure S5G).

To test the function of skeletal muscle at the whole-body level, we performed a maximal exercise capacity test using a motorized treadmill. The total distance traveled, time until exhaustion, and work performed significantly correlated with weight loss demonstrating a reduction in exercise capacity in mice with CACS (Figure 2E). Blood lactate levels after

exercise were similar in both groups suggesting that the mice with CACS reach their lactate threshold at a lower workload (Figure 2F). Combined with the biochemical assessment of skeletal muscle enzyme activity, this result suggests that pyruvate is being diverted away from the TCA cycle and oxidative phosphorylation. Indeed, the steady-state abundance of the TCA intermediates citrate, fumarate, and malate were reduced (Figures 2G, 2H, and 2I). These studies reveal distinct metabolic changes that occur in the glycolytic skeletal muscles of mice with CACS that may limit spontaneous activity and forced exercise capacity.

Caloric restriction mirrors the energetic changes observed in CACS and distinctly alters adipose tissue and skeletal muscle metabolism.

In order to assess the contribution of reduced food intake to TEE and skeletal muscle metabolism, we performed an experiment where WT mice were calorie-restricted (CR) to consume the same energy (~8 kcal/day) as mice with CACS (Figure S6A). CR led to similar changes in weight, body composition, TEE, and VO2 as CACS (Figures 3A, 3B, 3C, and S6B). RER was lower than control WT mice, except for the 3 hour period after the food was given (Figure S6C). Remarkably, CR induced a 4-fold increase in spontaneous activity, which has been previously described as “food-seeking behavior” [18] (Figure 4D). We estimated the REE, AEE, and caloric cost of activity (CCA) of the WT, tumor-bearing, and CR mice using a penalized spline regression [19] on the indirect calorimetry data (Figure S7). From this analysis, we observed significant reductions in REE in the CACS and CR mice in comparison to WT mice and mice without CACS. The significant increase in spontaneous activity in the CR mice led to a significant change in

AEE between CR and CACS. There was a trend for CCA to be lower in CR mice as compared to WT, suggestive of improved work efficiency [20,21].

Similar to CACS, CR reduced the mass of gWAT, BAT, and glycolytic (but not oxidative) skeletal muscles (Figures S8A and S8B). Histologically, the gWAT and skeletal muscle displayed atrophy with small adipocytes and reduced fiber cross-sectional area, respectively (Figure S8C). Contrary to what was observed in mice with CACS, the BAT of CR mice was depleted of lipid droplets. Moreover, the UCP1 tissue staining was more intense in the BAT and only identified in rare patches in the gWAT of CR mice (Figure S8D).

The changes in skeletal muscle were also unique following CR. The PFK activity tended to increase in both the Soleus and EDL (Figure 3E). Moreover, the citrate synthase activity was significantly higher in EDL muscles of CR mice (Figure 3F) without changes in the abundance of the electron transport chain proteins (Figure S8E). These changes in skeletal muscle metabolism were associated with improved distance traveled during an exercise performance test (Figure 3G), however, the work performed was similar given their lower body weight (Figure 3H). If we consider CR mice as a control for chronic anorexia, these data reveal distinct changes in adipose tissue browning and skeletal muscle metabolism that occur in CACS, a condition with similar food intake, body composition, and TEE.

Targeting GDF15 and activin A does not improve CACS in KL mice.

It is unclear what drives anorexia and the changes in peripheral organ metabolism in KL mice with CACS. In other cachexia models, GDF-15 induces anorexia through activation of a brainstem "sickness center" [22–26]. Also, Activin-A, a ligand of the ActRIIB receptor, can induce skeletal muscle atrophy and modulate adipocyte browning [25,27,28]. We checked the levels of both proteins and saw that they were specifically increased in the serum of mice with CACS in comparison to WT mice, KL mice without CACS, and CR mice (Figures 4A and 4B).

Therefore, we sought to inhibit the action of these proteins using monoclonal antibodies (mAb) and test the effects on food intake, TEE, and survival. Before testing the mAbs in tumor-bearing mice, we performed a pilot study to test their safety. WT mice were treated with IgG control (20 mg/kg, QW, SQ), anti-GDF15 mAb (10 mg/kg, QW, SQ) alone, or a combination of anti-GDF15 mAb and ActRIIB-Fc (20 mg/kg, QW, SQ), for 2 weeks. Food intake, body weight, and lean mass were significantly increased with the combination therapy (Figures S9A, S9B, S9C), and fat mass was subtly reduced in the IgG and anti-GDF15 treated mice (Figure S9D). No alterations were observed in EE, VO2, RER, and activity among the treatment arms (Figures S9G, S9H, S9I, and S9J) leading to the overall conclusion that these mAbs were safe in mice of this genetic background.

We proceeded with a prospective RCT in a cohort of KL mice. Mice were induced with AdCre and then monitored weekly for changes in body weight and food intake. Once the mice reached 15% weight loss, they were randomized to one of the 3 intervention arms. There was no difference in the weight loss at the start of treatment (Week 0) among the

arms, as expected (Figure 4C). After the first week of treatment, the mice treated with the combination of anti-GDF15 mAb and ActRIIB-Fc had significantly less weight loss than mice treated with the control IgG (Figure 4C). This trend persisted at week 2 of treatment however did not reach statistical significance because many of the IgG-treated mice reached euthanasia criteria (30% weight loss) after 1 week of treatment. Therefore, we compared the changes in body weight among groups at the “End” of treatment, which was defined as the date of euthanasia. In this assessment, the mice treated with the combination therapy showed a significant attenuation in weight loss (Figure 4D). This response was mostly driven by two female mice where CACS was reversed. The combination therapy also protected against the loss of glycolytic skeletal muscles but not oxidative muscles or adipose tissue (Figures 4E, 4F, S10A, S10B, and S10C). There were no changes in overall survival, EE, and activity by either treatment (Figures 4G, 4H, and 4I), as well as in food intake, VO2, and RER (Figures S10D, S10E, and S10F).

Anamorelin and ActRIIB-Fc combination treatment improves weight, activity, and overall survival in KL mice with CACS.

Anamorelin hydrochloride was recently approved by the pharmaceutical regulatory authority of Japan for the treatment of patients with CACS [29]. Anamorelin is a non-peptide ghrelin receptor agonist that has been reported to induce food intake and improve survival in patients with CACS [30–32]. Therefore, we planned a prospective RCT in KL mice using anamorelin fumarate (Ana) and ActRIIB-Fc. This combination therapy was determined to be safe in a pilot study of WT mice (data not shown). Using a similar design as the GDF15

trial, we randomized KL mice into 3 intervention arms (Control, Ana, or Ana + ActRIIB-Fc). Mice treated with Ana + ActRIIB-Fc showed a significant increase in food intake and weight loss after 2 weeks of treatment (Figures S11A and S11B). The combination therapy also protected against the loss of fat and lean mass (Figures S11C and S11D). There were no changes in overall survival and EE by either treatment (Figures S11E, S11F, and S11G); however, spontaneous activity was restored in the mice treated with Ana + ActRIIB-Fc (Figure S11H) and the gastrocnemius, a primarily glycolytic muscle, was protected (Figures S11I and S11J).

During this trial, we noticed that female mice seemed to respond better than male mice. Therefore, we stratified the cohort by gender and interrogated the therapeutic efficacy of these interventions. In this analysis, it was clear that male mice did not benefit from either intervention (Figures S12). However, there was a strong effect in female mice. Ana significantly increased food intake, weight, and fat mass in the female mice (Figures 5A-C). The addition of ActRIIB-Fc to Ana further improved weight due to an increase in lean mass (Figures 5B and 5D). Remarkably, CACS was fully reversed in two-thirds of the female mice treated with the combination of Ana and ActRIIB-Fc without changes in lung mass, a surrogate for tumor burden (Figure 5E). The combination therapy restored spontaneous activity and improved overall survival (Figures 5E and 5F).

Discussion

In this study, we performed a comprehensive analysis of the changes in food intake, peripheral organ metabolism, and TEE that occur in mice following induction of lung

cancer. We show that KL mice with CACS have anorexia and suppressed TEE. The reduction in TEE is more than what is predicted by changes in lean mass alone. This physiologic adaptation to weight loss has been observed in other mouse models of CACS and humans undergoing CR [33,34]. In this setting, the TEE reduction is due, in part, to reduced skeletal muscle glycolytic metabolism and improved work efficiency that can be prevented with low-dose leptin treatment [35,36]. Similarly, KL mice with CACS have atrophy of glycolytic muscle fibers [11], reduced muscle PFK activity, and low levels of leptin; these changes may improve muscle efficiency and contribute to the decrease in TEE during CACS.

Low levels of leptin are also known to contribute to the dramatic increase in spontaneous activity that we observed in mice following CR. This phenomenon has been previous described as “food-seeking behavior” or “semi-starvation–induced hyperactivity” and it can be suppressed by replacing leptin or increasing housing temperature [37,38]. We find that mice with CACS do not display hyperactivity despite the presence of anorexia, hypoleptinemia, and low housing temperature. In fact, spontaneous activity is reduced in KL mice with CACS. Interestingly, we find that increasing the housing temperature normalizes activity in mice with CACS. These data suggest that the neurohormonal pathways regulating thermogenesis may suppress spontaneous activity in mice with CACS.

Our data highlights the dramatic changes that occur to adipose tissue during CACS. KL mice develop increased rates of lipolysis, browning, and atrophy of the WAT adipocytes. Data from other mouse models and human studies of CACS show that WAT lipolysis is

an essential feature of CACS [22,39,40], however, the role of browning is more controversial. In certain models, browning exacerbates the negative energy state [9,41], but this finding is not consistent with clinical studies in subjects with lung cancer nor our data from the KL mice [42–49]. We speculate that the browning observed in KL mice with CACS occurs in response to an increased demand for thermogenesis following the loss of the abdominal "insulation" provided by skeletal muscle and adipose tissues. Furthermore, we identified histologic and biochemical evidence of BAT dysfunction in mice with CACS. The BAT lipid droplets were found to be enlarged and associated with reduced UCP1 mRNA expression and protein abundance consistent with *whitening* of the BAT. This phenotype has been observed in mouse models of diet-induced obesity where it can be reversed with fenofibrate, a PPARα-agonist [50,51]. Interestingly, we previously showed that fenofibrate can prevent CACS in KL mice so the role of BAT in this syndrome needs further study [11,50,51].

Our results identify the distinct alterations in skeletal muscle metabolism that occur during weight loss from CACS in comparison to weight loss from CR. In both conditions, we see similar reductions in body weight, skeletal muscle mass, and TEE; however, the reduction in exercise tolerance and markers of oxidative metabolism only occur in CACS. It is unclear if the lack of spontaneous activity and limited exercise tolerance is due to malaise (*i.e.* CNS-mediated) or a primary deficit in skeletal muscle. In support of the latter, Kamei et al. have shown that overexpression of Forkhead box protein O1 (FoxO1) in skeletal muscle is enough to suppress spontaneous activity, and we have previously shown that the muscles from KL mice with CACS have increased expression of this protein [52]. We

also found evidence for a reduction in the gene expression and protein abundance of several proteins involved in the electron transport chain in the EDL of mice with CACS; however, there was no change in the oxygen flux of the permeabilized EDL when measured *ex vivo*. Given that the EDL contains significant numbers of non-atrophied type IIA fibers [11], we speculate that the activity of these highly oxidative fibers is masking any change in *ex vivo* oxygen flux.

In an attempt to treat anorexia and the loss of skeletal muscle mass during CACS, we treated KL mice with an anti-GDF15 mAb alone or in combination with an ActRIIB-Fc mAb, which induces hypertrophy of glycolytic muscle fibers [53]. Both GDF15 and Activin A are elevated in mouse models and humans with CACS [54–57], and the systemic inhibition of either signaling pathway can prevent CACS in other mouse models [22,24,58–60]. However, we did not observe significant improvements in food intake or TEE with either treatment. This result may be due to the overall low abundance of GDF15 in the KL mice as compared to other models where anti-GDF15 therapy has shown benefit [22,24,60]. While the addition of ActRIIB-Fc to anti-GDF15 did not improve food intake, it did significantly delay the progression of CACS and preserve skeletal muscle mass. More importantly, we find that the combination of Ana with ActRIIB-Fc significantly improved body composition, activity, and overall survival. The degree of survival improvement we observed is on par with the effects of chemotherapy and immunotherapy in this model [61,62].

The beneficial effects of Ana and ActRIIB-Fc were limited to female mice. We have a limited understanding of the basic mechanisms underlying sex differences in CACS [63].

There are known differences in body composition, EE, and peripheral organ metabolism between men and women [64]. Gender discrepancies have also been observed in animal models of disuse atrophy and cardiac cachexia [65–67]. Additional studies are required to identify the key pathophysiologic differences that drive the differential therapeutic response between male and female KL mice.

Our data show that CACS in female mice with lung cancer can be overcome by stimulating appetite and blocking catabolic activin signaling. There are late-stage clinical compounds available for the immediate translation of our findings. Anamorelin was recently approved by the pharmaceutical regulatory authority of Japan for the treatment of patients with CACS, and bimagrumab, a fully human monoclonal antibody that prevents ligand binding to ActRIIB, is safe and increases lean mass in adults with sarcopenia [29,68]. Despite the improvement in lean mass, these patients did not show any benefits on physical function and overall survival. Our data suggests that a combination of multimodal, gender-specific, therapies are needed for effective reversal CACS.

Acknowledgments

This work was supported by a grant from the Lung Cancer Research Foundation (M.D.G.), NIH K08 CA230318 (M.D.G.), NIH R35 CA197588 (L.C.C.), and institutional support from Weill Cornell Medicine. We thank the Metabolic Phenotyping Center, the WCM Proteomics and Metabolomics Core Facility, the Electron Microscopy and Histology Core Facility, the Vanderbilt Mouse Metabolic Phenotyping Center (NIH DK059637) and Diabetes Research and Training Center (NIH DK020593), the Louisiana Clinical and Translational Science Center (U54 GM104940) and the Scott Rodeo for use of the rodent treadmill. The GDF15 antibody, Anamorelin, and ActRIIB-Fc antibody were provided by Pfizer, Inc. Catecholamines assays were performed by the VUMC Hormone Assay and Analytical Services Core which is supported by NIH grants DK059637 and DK020593.

Author Contributions

A.L.Q., S.R., E.D., E.R.M.Z., R.J.L., C.J.M., C.D.H., C.L.A., and M.D.G. performed experiments. A.L.Q., S.R., E.D., E.R.M.Z., R.J.L., C.J.M., C.D.H., C.L.A., Z.W., D.E.C., L.C.C., and M.D.G. designed the project. A.L.Q., E.D., E.R.M.Z., C.J.M., C.D.H., J.P.K, C.L.A., G.G., and M.D.G analyzed the data. A.L.Q and M.D.G. wrote the paper. All authors read, edited, and approved the manuscript.

Declaration of Interests

L.C.C. is a founder, shareholder, and member of the scientific advisory board of Agios Pharmaceuticals and a founder and former member of the scientific advisory board of Ravenna Pharmaceuticals (previously Petra Pharmaceuticals). These companies are developing novel therapies for cancer. L.C.C. has received research funding from Ravenna Pharmaceuticals. M.D.G. reports personal fees from Novartis, Petra Pharmaceuticals, and Bayer. He has received research support from Pfizer Inc. L.C.C. and M.D.G. are inventors on patents (pending) unrelated to the scope of the current work. L.C.C. and M.D.G. are co-founders and shareholders in Faeth Therapeutics. Z.W. is a full-time employee of Pfizer Inc. All other authors report no competing interests.

Figure Legends

Figure 1. Energy Expenditure is Reduced during CACS and Not Altered by Thermoneutrality WAT atrophy during CACS is associated with higher lipolysis and browning. (A) Lean mass and (B) Fat mass measured early (4 weeks after induction), mid (when mice reached 15% weight loss), and late (before euthanasia) stages of the disease. (C-F) Wild-type (WT) and tumor-bearing KL mice were housed under 22°C or 30°C in metabolic cages (N = 4-16). (C) Hourly energy expenditure (kcal/h) of non-cachexic (-CACS) and cachexic (+CACS) mice over a representative 24 hour period; (D) Total daily energy expenditure versus total body lean mass for WT, -CACS, tumor-bearing mice without weight loss that later developed CACS (Pre-CACS), and +CACS. Linear regression is plotted WT (black) and +CACS (red) mice; (E) Cumulative food intake (kcal) of -CACS and + CACS over a representative 24 hour period; (F) Cumulative activity (m) of -CACS and + CACS over a representative 24 hour period; Graphs show mean ± SEM. B/D/E comparisons made by 2way ANOVA with post-test compared to -CACS or -CACS 30°C mice: $*P < 0.05$.

Figure 2. Mice with CACS have impaired skeletal muscle metabolism. (A) Phosphofructokinase (PFK) activity measured using lysates from Soleus and extensor digitorum longus (EDL) muscles from mice without (-CACS) and with cachexia (+CACS); (B) Western blot of phosphorylated (Tyr10) and total LDHa, phosphorylated (Ser293) and total PDHe1α, and Tubulin from Soleus and EDL lysates from -CACS and +CACS mice; (C) Relative mitochondrial DNA content in Soleus and EDL muscles of -CACS and +CACS mice; (D) Western blot analysis of mitochondrial oxidative

phosphorylation complexes (CI-subunit NDUFB8, CII-SDHB, CIII-UQCRC2, CIV-MTCO1, and CV-ATP5A) as well as VDAC, GAPDH, and Tubulin in lysates of Soleus and EDL muscles from -CACS and +CACS mice; (E) Distance traveled (m), work performed (J), and duration (min) of maximal endurance performance test (running on a treadmill until exhaustion) of KL mice versus total body weight loss. Linear regression of each metric is shown; (F) Blood lactate levels of -CACS and +CACS mice at the completion of the maximal endurance performance test in E; (G) Citrate, (H) Fumarate, (I) Malate metabolite levels in gastrocnemius extracts from -CACS and +CACS mice. Graphs show mean ± SEM. A/C/F/G/H/I comparisons made using Student's t-test compared with -CACS mice: *P <0.05. E comparison was made using correlation analysis (R, Pearson r, and p, P value).

Figure 3. Calorie restriction mirrors the energetic changes observed in CACS except for activity and distinctly alters adipose tissue and skeletal muscle metabolism. Wild-type mice were calorie restricted (CR) by feeding a ~8 kcal/day diet (amount consumed by cachectic mice) until weight stabilization. (A) Percent of initial body weight over a period of 18 days of CR; (B) Total body, Fat, and Lean mass of mice in A at day 18; (C) Total daily energy expenditure (kcal) in 24 hour; (D) Cumulative activity (m) over a representative 24 hour period. (E) Phosphofructokinase (PFK) activity and (F) Citrate synthase activity measured using lysates from Soleus and EDL muscles; (G) Distance traveled (m) and (H) Work (J) performed by Fed CR mice performing a maximal endurance performance test (running on a treadmill until exhaustion). Graphs show mean ± SEM. A/B//E/F/G/H comparisons made using Student's t-test compared

with -CACS mice and D by 2way ANOVA with post-test compared with Fed mice. *P <0.05.

Figure 4. GDF-15 and ActRII-Fc mAb combination treatment in KL mice. (A) Serum GDF15 levels from wild-type mice (Fed or calorie restricted [CR]) and tumor-bearing mice without (-CACS), or with cachexia (+CACS) at the time of euthanasia; (B) Serum Activin A levels in mice from A; (C) Total body weight loss (%) over the period of 4 weeks following randomization to treatment with either control immunoglobulin (IgG), anti-GDF15 monoclonal antibody (mAb) or anti-GDF15 mAb together with a decoy ActRIIB-Fc mAb. Mice were randomized and treatment was started following tumor induction once the mice reached 15% weight loss; (D) Weight loss (%) at Week 0 (Start) and after 2 weeks (End) of treatment in mice from C; (E) extensor digitorum longus (EDL) and (F) gonadal white adipose tissue (gWAT) mass from mice in C; (G) Overall Survival (Weeks from induction) of mice in C; (H) Hourly energy expenditure (kcal/h) and (I) Cumulative activity (m) of mice in C over a representative 24 hour period. Graphs show mean ± SEM. A/B comparisons made by 2way ANOVA compared with Fed mice: *p <0.05. C comparison made using Student's t-test compared to IgG-treated mice at week 1 of treatment: *p <0.05. D comparison made by Student's t-test between Start and End of each treatment: *p <0.05. E comparisons made by 2way ANOVA with post-test compared with Fed mice: *p <0.05.

Figure 5. Anamorelin fumarate and ActRIIB-Fc combination treatment improved overall survival and protected KL mice from skeletal muscle loss. (A) Food intake (kcal/d) at week 0 (Start) and after 2 weeks (End) of treatment. (B) Weight loss (%) at

week 0 (Start) and after 2 weeks (End) of treatment; Fat (C) and Lean (D) mass (%) measured after 2 weeks of treatment; (E) Lung wet mass (mg) at the time of euthanasia; (F) Cumulative activity (m) of mice in C over a representative 24 hour period; (G) Overall survival (weeks from induction). Graphs show mean ± SEM. A/B/C/D/E comparison made by Student's t-test: *p <0.05. F comparison made by 2way ANOVA compared with Control: *p <0.05 and Ana: $^{\#}$p <0.05.

Figure S1. CACS-induced WAT atrophy is associated with higher lipolysis and browning. (A) Gonadal white adipose tissue (gWAT) and (B) interscapular Brown adipose tissue (BAT) mass versus the percentage of total weight loss; (C) H&E staining of interscapular brown adipose tissue (BAT) and gonadal white adipose tissue (gWAT) from wild-type (left), non-cachectic (-CACS, center), and cachectic (+CACS, right) mice; (D) Principal component analysis using RNA Seq data from +CACS (pink) and -CACS (green) gWAT; (E) Deconvolution analysis to identify BAT and gWAT-specific genes (BATLAS) from -CACS and +CACS gWAT RNA Seq. Bar graphs show the proportion of BAT gene enrichment; (F) Uncoupling protein 1 (UCP1) immunohistochemistry (IHC) of BAT and gWAT from representative wild-type (WT, left), -CACS (center), and +CACS (right) mice; (G) Western blot analysis of PGC1α and GAPDH from gWAT lysates from -CACS and +CACS mice (top) and PGC1α, UCP1 and GAPDH from BAT lysates from -CACS and +CACS mice (bottom); (H) Relative mRNA expression of *Ucp1*, *Lep* and *Ppargc1*α from gWAT and (I) BAT from -CACS and +CACS mice; (J) Serum leptin levels from -CACS and +CACS mice at the time of euthanasia; (K) Triacylglycerol (TG) release from dissected gWAT from non-cachexic (-CACS) and cachexic (+CACS) mice

following *ex vivo* incubation in the presence or absence of Isoproterenol (Iso) over a period of 120 minutes; (L) Non-esterified fatty acids (NEFA) measured in -CACS and +CACS mice at the time of euthanasia. Graphs show mean ± SEM. A/B by Student's t-test; C/D by correlation analysis (R, Pearson r, and p, *P* value): **P* <0.05. E/H/I/J comparisons made by Student's t-test compared with -CACS mice: *p <0.05. K comparison by 2-way ANOVA with post-test compared to -CACS group. L comparison by one-way ANOVA with post-test compared to -CACS: *p <0.05.

Figure S2. Additional measures from mice under thermoneutrality. Non-cachexic (-CACS) and cachexic (+CACS) mice were housed under 22°C or 30°C in metabolic cages (N = 4-16). (A) Hourly volume of oxygen consumed (ml/h) and (B) respiratory exchange ratio (RER) of -CACS and +CACS mice over a representative 24 hour period; (C) Weight normalized to the peak value following induction of lung cancer when housed at 22°C or 30°C (N= 9/male and 12/female); (D) Overall Survival of mice from C. Graphs show mean ± SEM.

Figure S3. Hormonal alterations in CACS-induced mice. Serum hormone levels from non-cachexic (-CACS) and cachexic (+CACS) mice. (A) Corticosterone; (B) Norepinephrine; (C) Epinephrine; (D) triiodothyronine (T3); (E) thyroxine (T4); (F) Insulin. Graphs show mean ± SEM. A comparison made by Student's t-test compared with -CACS mice: *p <0.05.

Figure S4. Skeletal muscle mass of KL mice. (A) Gastrocnemius (Gastro) and Quadriceps (Quad), and (B) Soleus and EDL mass of KL mice versus weight loss (% from peak weight). Correlation analysis (R^2, Linear regression, and p, *P* value).

Figure S5. Additional changes in skeletal muscle of KL mice. (A) Principal component analysis of gastrocnemius RNA Seq data obtained from cachexic (+CACS, pink) and non-cachexic (-CACS, green) mice; (B) Pathway enrichment analysis of the differentially expressed genes identified in A. Peak plot of enriched pathways is indicated over enrichment distribution. The color of the peaks represents the range of *P*-adjusted values; (C) Representative electron micrograph of extensor digitorum longus (EDL) and Soleus muscles taken from -CACS (left) and +CACS (right) mice; (D-E) oxygen flux (OXPHOS) and electron transport (E) capacity of permeabilized Soleus and EDL fibers (-CACS N=14, +CACS N=19). (D-E) Oxidative phosphorylation (OXPHOS) and electron transfer (E) capacity of permeabilized Soleus and EDL fibers (-CACS N=14, +CACS N=19). NADH-linked (N) LEAK (L) respiration was measured in the presence of pyruvate and malate (PM_L or PM_P) and absence of ADP. N-linked OXPHOS (P) was then determined by addition of ADP and glutamate (PMG). The combined effect of N and Succinate-linked (S) respiration was then determined by addition of succinate in the presence of PMG ($PMGS_P$). The mitochondrial uncoupler FCCP was added to facilitate maximal E in the presence of PMGS ($PMGS_E$). TMPD and ascorbate were then added to measure maximal ET through complex IV (CIV_E); (F) Citrate synthase activity measured in soleus and EDL muscles of mice with and without CACS; (G) T3 and T4 levels measured in gastrocnemius muscle of mice with or without CACS. Data are shown as the mean ± SEM. Panels D and E were assessed by two-way ANOVA with Tukey's multiple comparisons.

Figure S6. Additional changes in CR mice. Wild-type mice were calorie restricted (CR) by feeding a ~8 kcal/day diet (amount consumed by cachectic mice) until weight stabilization. (A) Cumulative food intake (kcal) over a representative 24 hour period; (B) Hourly volume of oxygen consumed (ml/h) over a representative 24 hour period; (C) Hourly respiratory exchange ratio (RER) over a representative 24 hour period. Graphs are mean ± SEM. B comparison made using 2way ANOVA compared with Fed mice: *p <0.05.

Figure S7. Alterations in energy expenditure-related parameters in KL mice. Alterations in energy expenditure-related parameters in wild-type (WT), mice without CACS (-CACS), mice with CACS (+CACS), and caloric-restricted (CR) mice. (A) Daily Resting energy expenditure; (B) Daily Activity energy expenditure; (C) Caloric cost of activity. Graphs show mean ± SEM. A/B comparisons made using 2way ANOVA compared within all groups of mice: *p <0.05.

Figure S8. Caloric restriction. Wild-type mice were calorie restricted (CR) by feeding a ~8 kcal/day diet (amount consumed by cachectic mice) until weight stabilization. (A) Gonadal white adipose tissue (gWAT) and interscapular Brown adipose tissue (BAT) mass of WT (Fed) and mice following CR; (B) Gastrocnemius (Gastro), quadriceps (Quad), tibialis anterior (TA), extensor digitorum longus (EDL), and Soleus muscle wet mass (mg) at the time of euthanasia; (C) H&E staining of Fed mice gonadal white fat (gWAT) (top, left), CR gWAT (bottom, left), Fed interscapular brown adipose tissue (BAT) (top, center), CR BAT (bottom, center), Fed quadriceps (Quad) (top, right), CR Quad (bottom, right); (D) Uncoupling protein 1 (UCP1) immunohistochemistry staining

of a representative gWAT (left) and BAT (right) removed from Fed and CR mice; (E) Western blot analysis of mitochondrial oxidative phosphorylation complexes (CI-subunit NDUFB8, CII-SDHB, CIII-UQCRC2, CIV-MTCO1, and CV-ATP5A) in Soleus and (F) EDL muscles of Fed and CR mice. Graphs show mean ± SEM. A/B/E comparisons made using Student's t-test compared with -CACS mice: *P <0.05.

Figure S9. Pilot study: GDF-15 and ActRII-Fc mAb combo treatment in WT mice. (A-H) Wild-type (WT) mice were treated either with control immunoglobulin (IgG), anti-GDF15 monoclonal antibody (mAb), or anti-GDF15 mAb together with a decoy ActRIIB-Fc mAb for 2 weeks (N=8 per group). (A) Daily food intake; (B) Weight change (% from initial); (C) Lean mass (%) (% from initial); (D) Fat mass (%) (% from initial); (E) Hourly energy expenditure (kcal/h), (F) Hourly volume of oxygen (ml/h) consumed, (G) Respiratory exchange ratio (RER), and (H) Cumulative activity (m) over a representative 24 hour period. Graphs show mean ± SEM. A/B/D comparisons made by 2way ANOVA compared within all groups of mice: *p <0.05.

Figure S10. Additional changes in +CACS mice treated with GDF-15 and ActRII-Fc mAb combination. (A-F) Mice with cachexia (CACS) treated either control immunoglobulin (IgG), anti-GDF15 monoclonal antibody (mAb), or anti-GDF15 mAb together with a decoy ActRIIB-Fc mAb for a maximum of 4 weeks. (A) Quadriceps (Quad) mass; (B) Brown adipose tissue (BAT) mass; (C) Soleus mass; (D) Daily food intake; (E) Hourly volume of oxygen (ml/h) consumed over a representative 24 hour period; (G) Respiratory exchange ratio (RER) over a representative 24 hour period.

Graphs show mean ± SEM. A comparison made by Student's t-test compared with IgG mice: *p <0.05.

Figure S11. Effect of Ana and ActRIIB-Fc combination treatment in male and female mice. (A) Food intake (kcal/d) at week 0 (Start) and after 2 weeks (End) of treatment. (B) Weight loss (%) at week 0 (Start) and after 2 weeks (End) of treatment; Fat (C) and Lean (D) mass measured after 2 weeks of treatment; (E) Lung wet mass (mg) at the time of euthanasia; (F) Overall survival (weeks from induction); (G) Hourly energy expenditure over a representative 24 hour period; (H) Cumulative activity (m) of mice over a representative 24 hour period; (I) Fat tissues weight measured at the time of euthanasia (J) Muscle tissues weight measured at the time of euthanasia. Graphs show mean ± SEM. A/B/C/D comparison made by Student's t-test: *p <0.05. H comparison made by 2way ANOVA compared with Control: *p <0.05 and Ana: $^{\#}$p <0.05. J comparison by one-way ANOVA with post-test compared to -CACS: *p <0.05.

Figure S12. Anamorelin fumarate and ActRIIB-Fc combination treatment in KL male mice. (A) Food intake (kcal/d) at week 0 (Start) and after 2 weeks (End) of treatment. (B) Weight loss (%) at week 0 (Start) and after 2 weeks (End) of treatment; Fat (C) and Lean (D) mass measured after 2 weeks of treatment; (E) Total daily energy expenditure (kcal) in 24 hour period; (F) Cumulative activity (m) of mice over a representative 24 hour period; (G) Overall survival (weeks from induction). Graphs show mean ± SEM. F comparison made by 2way ANOVA compared with Control: *p <0.05.

Methods

Experimental Model

$Kras^{G12D/+}$; $Lkb1^{f/f}$ mice have been previously described [69]. Mice were housed in a 12-h light/dark cycle at 22 °C or 30 °C ambient temperature and received rodent chow (PicoLab Rodent 20 5053; Lab Diet) and free access to drinking water. Tumors were induced in adult (12- to 20 week-old) mice via intranasal administration of 75 μL of PBS containing 2.5×10^7 pfu of Adenovirus CMV-Cre (Ad5CMV-Cre) obtained from the University of Iowa Gene Transfer Vector Core (Iowa City, IA) and 1 mM CaCl2.

Method Details

Tissue Collection. Whole blood glucose was measured using a point of care glucose meter and blood from the tail vein before CO2 asphyxiation. Following euthanasia, whole blood was collected via cardiac puncture and placed into pre-treated tubes for serum/plasma isolation. Next, the liver, gonadal adipose, kidney, and skeletal muscles (gastrocnemius, quadriceps, tibialis anterior, EDL, and Soleus) were dissected, weighed, and flash-frozen in liquid nitrogen. All tissues were subsequently stored at −80 °C until further processing.

Metabolic Cage Analyses. Mice were individually housed at 22 or 30 °C and subjected to indirect calorimetry for a period of 3 consecutive days under a 12h light-dark cycle. During this period, we measured food and water intake, spontaneous activity, and volume of oxygen and carbon dioxide consumed. This data allows us to estimate total energy expenditure (TEE) and the respiratory exchange ratio (RER). We recorded the KL mice in two phases: 1- Acclimation, first 24 hours of measurement; 2- Fed, 24 hours after the end of phase 1, mice were fed ad libitum. A penalized spline regression model [19] was used to estimate the resting energy expenditure (REE), activity energy expenditure (AEE), and caloric cost of activity (CCA). To calculate CCA, we fit a simple linear regression model between activity rate and total energy rate for each mouse. The slope of each line is the CCA for each respective mouse. To calculate AEE, the mouse's activity rate was multiplied by its CCA. REE was calculated by subtracting AEE from TEE. REE and AEE were then smoothed using a second-order polynomial smoothing spline. This method allows for the calculation of AEE while taking into account time-varying REE.

Body Composition Analysis. Mice were weighed, and body composition (fat mass, free fat mass, and water mass) was measured using an EchoMRI-100H 2n1 with a horizontal probe configuration (EchoMRI, Houston, TX).

Exercise capacity test. Mice were acclimated (30 min at 8m/min) to a motorized treadmill one week before the maximal exercise capacity test. Shocking grids with frequency set at: 75 per minute and intensity at: 45% (3.4mA) were located at end of the treadmill to force the mice to run at their maximum. On the day of the test, the protocol was initiated with 3 min acclimation without any speed. Start speed was set to 8m/min followed by incremental adjustments of 2.5m/min every 3 minutes until fatigue was reached. Fatigue was defined as the mouse being stationary on the shocking grid for 20 seconds with no attempts to climb off the treadmill. Maximum speed, time and laps were then recorded and used to calculate, total time, total distance, and work. Lactate was quantified before and after the exercise protocol using a point of care device (Nova Biomedical).

Therapeutic trials. Drugs were provided by Pfizer (Boston, USA)and have been previously described [70,71]. A pilot experiment was performed to assess safety in 24 WT mice. The mice were randomly assigned into 3 groups: IgG control (20 mg/kg, QW, SQ), a weekly injection of GDF15 mAb (10 mg/kg, QW, SQ) alone, or a combination of GDF15 mAb and ActRIIB-Fc (20 mg/kg, QW, SQ), for 2 weeks. Anamorelin fumarate (Ana) was obtained from BOC Sciences (New York, USA). Next, we performed 2 prospective, randomized, controlled, intervention trials using KL tumor-bearing mice (RCT 1 and RCT2). RCT1 was performed using mAb against GDF15 alone or in combination with ActRIIB-Fc. RCT2 was performed using Ana alone or in combination with ActRIIB-Fc. Analysis of data from our previous cohorts determined that 7 mice per group were required to detect a 20% change in mean weight loss (α=0.05, β=0.9) in tumor-bearing mice. In order to account for early mortality and the proportion of mice without CACS, a total of 39 mice (22 males, 17 females) were induced. Of those, 30 mice (18 males, 12 females) reached 10-15% weight loss and underwent randomization. The randomization was performed in blocks of 6 and stratified by gender [72]. The pre-specified primary outcome was the percent weight loss at 2 weeks following the start of treatment. Secondary outcomes included weight loss at the time of euthanasia, overall survival, body composition, food intake, spontaneous activity, skeletal muscle mass, and white adipose tissue mass.

Serum and Tissue Metabolites. Blood was centrifuged (10,000 × g for 10 min at 4 °C), and the serum or plasma was stored at −20 °C. Serum β-hydroxybutyrate, TG (Stanbio Laboratory), and NEFA (Wako Life Sciences) were determined using commercially available kits. Serum insulin, corticosterone (APLCO Diagnostics), Leptin (Milipore, cat.# EZML-82K), Activin-A (DAC00B, R&D Systems), GDF-15 (MGD150, R&D Systems) levels were quantified by ELISA. Plasma epinephrine and norepinephrine were measured by HPLC via chromatography data station [73,74] by the Vanderbilt Hormone and Analytical Services Core (sensitivity of 0.5 ng/ml for the mouse samples). Serum T3 and T4 were determined by radioimmunoassay in a double antibody technique. T4 was measured by using I125-labeled T4 (MP Biomedicals Cat# 06B257231) and 1st antibody developed in rabbit (Sigma Cat# T2652). T3 was measured by using I125-labeled T3 (MP Biomedicals Cat# 06B254282) and 1st antibody developed in rabbit Sigma Cat# T2777). Tissue metabolites (including T3 and T4) were extracted from gastrocnemius (whole muscle) using 80% methanol [75]. Targeted LC/MS analyses were performed on a Q Exactive Orbitrap mass spectrometer (Thermo Scientific) coupled to a Vanquish UPLC system (Thermo Scientific) as previously described [11]. Metabolites were identified on the basis of exact mass within 5 ppm and standard retention times. Relative metabolite quantitation was performed based on the peak area for each metabolite. All data analyses were done using scripts written in-house by the WCM Proteomics and Metabolomics Core Facility.

RNA Sequencing and Analysis. Total RNA was extracted from gastrocnemius (whole muscle) and gonadal WAT (whole depot) using TRIzol (Thermo Fisher), followed up by a clean-up step using RNeasy kit (Qiagen). One microgram of total RNA of each sample was submitted to the WCM Genomics Resources Core Facility. Raw sequenced reads were aligned to the mouse reference GRCm38 using STAR (v2.4.1d, 2-pass mode) aligner and Raw counts were obtained using HTSeq (v0.6.1) [76,77]. The principal component analysis (PCA) was performed using R Studio Version 3.6.3 and DEBrowser shiny application [78]. Genes with <10 CPM were filtered out and batch effect correction was achieved using the Combat method [79]. The differentially expressed genes (DEG) were obtained using DESeq2 and were considered statistically significant when FDR < 0.05 and Log2(FC) > 1.5. The list of DEG was then used for KEGG pathway enrichment analysis using the R package clusterProfiler [80]. The probability of browning in the WAT was assessed using the online webtool BATLAS [13].

RT-qPCR. Total RNA was extracted from total muscle EDL and Soleus using the above method and cDNA was synthesized using SuperScript VILO Master Mix. cDNA was amplified using the Applied Biosystems TaqMan Gene Expression Assays (Thermo

Fisher) with primers for the following genes: Ucp1; Lep; Rer1 and Actb. cDNA was amplified using the Applied Biosystems SYBR™ Select Master Mix (Thermo Fisher) with primers for the following genes: Ppargc1a, Tbp, and Actb. Relative mRNA content was determined using the ΔΔCt method.

Mitochondrial DNA. Total DNA was isolated from EDL and Soleus using Qiagen Dneasy Blood and Tissue Kit and treated with RNase A according to the manufacture's instructions. The mitochondrial DNA content (*mt-Nd2*, *NADH dehydrogenase 2, mitochondrial*) relative to nuclear DNA (*Pecam1*, platelet/endothelial cell adhesion molecule 1) was determined by quantitative real-time PCR using the Applied Biosystems SYBR™ Select Master Mix (Thermo Fisher). Relative mtDNA content was determined using the ΔΔCt method.

Histology. gWAT and quadriceps were fixed with 4% paraformaldehyde solution in PBS and were embedded into paraffin. Four-micrometer sections were cut for staining with H&E. Samples were also stained for UCP1 through immunohistochemistry using 1:200 dilution of a recombinant anti-UCP1 antibody [EPR20381] (ab209483) that we validated against UCP1 knockout tissue.

Western Blots and Antibodies. EDL and Soleus (whole muscle) were lysed using lysis buffer containing 50 mM Tris·HCl (pH 7.4), 150 mM NaCl, 1 mM EDTA, 10% glycerol, 1% Nonidet P-40, 0.5% Triton X-100, and 1 tablet (per 10 mL) of protease and phosphatase inhibitor. Protein extracts (50 µg) were separated by 4–12% NuPAGE Bis-Tris or 4–20% NuPAGE Tris-Glycine gels and transferred to 0.45-µm PVDF membranes with wet transfer cells (Bio-Rad Laboratories). After 1 h of blocking with Tris-buffered saline with 0.1%(vol/vol) Tween 20 containing 3%(wt/vol) BSA (TBST), membranes were incubated overnight at 4 °C with antibodies against UCP1 (ab209483); PGC1 alpha (ab54481); LDHA (CST #2012); Phospho-LDHA (Tyr10) (CST #8176); Pyruvate Dehydrogenase (CST #3205); Anti-Pdhe1α (Ser293) (ab92696); Total OXPHOS Cocktail (ab110413); GAPDH (Proteintech 10494-1-AP), VDAC (CST #4661); and α-Tubulin (DM1A) (CST #3873) at a 1:1,000 dilution in 3% BSA followed by a TBST wash and the appropriate secondary antibody (1:10,000) for 1 h at room temperature. The signals were detected on HyBlot CL Autoradiography Film (Denville Scientific) with SuperSignal Western Blot enhancer solution (Thermo Fisher), scanned at 600 dpi resolution, cropped with Adobe Illustrator 2020 (Adobe).

Assessment of Oxidative Capacity in Permeabilized Muscle Fibers. Oxidative phosphorylation (OXPHOS) and electron transport (ET) capacity were determined *ex vivo* from permeabilized mixed gastrocnemius fibers as described previously [81]. Briefly,

intact soleus and EDL muscle was collected and immediately placed into BIOPS (50 mM K+-MES, 20 mM taurine, 0.5 mM dithiothreitol, 6.56 mM $MgCl_2$, 5.77 mM ATP, 15 mM phosphocreatine, 20 mM imidazole, pH 7.1, adjusted with 5 N KOH at 0 °C, 10 mM Ca–EGTA buffer, 2.77 mM CaK_2EGTA + 7.23 mM K_2EGTA; 0.1 mM free calcium) solution on ice. The muscle bundles were then mechanically separated under a dissection microscope, placed into fresh BIOPS containing saponin (5 mg/mL), and gently agitated at 4°C for 20 min. The fibers were then transferred to a mitochondrial respiration medium (MiR05; 110 mM sucrose, 60 mM K +-lactobionate, 0.5 mM EGTA, 3 mM $MgCl_2$, 20 mM taurine, 10 mM KH_2PO_4, 20 mM HEPES adjusted to pH 7.1 with KOH at 37 °C; and 1 g/l de-fatted BSA), blotted on filter paper, and weighed. 2-5 mg of permeabilized fiber bundles were transferred into the oxygraph chamber containing 2 mL of MiR05 until background respiration was stable. OXPHOS and ET capacity were measured using the following concentrations of substrates, uncouplers, and inhibitors: malate (2 mM), pyruvate (2.5 mM), ADP (2.5 mM), glutamate (10 mM), succinate (10 mM), tetramethyl-p-phenylenediamine (TMPD, 0.5 µM), ascorbate (2 mM), carbonylcyanide-p-trifluoromethoxyphenylhydrazone (FCCP, 0.5 µM increment), rotenone (75 nM), antimycin A (125 nM) and sodium azide (200 mM).

Electron Microscopy. Whole mouse EDL and soleus were dissected and pinned to a cork by the tendons at native length. The muscles were immediately fixed in 2.5% glutaraldehyde, 4% paraformaldehyde, 0.02% picric acid in 0.1M sodium cacodylate buffer, pH 7.3 overnight at 4 °C. Samples were washed with sodium cacodylate 0.1 M buffer then cut into small strips, maintaining fiber orientation and post-fixed with 1% OsO4-1.5%K-ferricyanide buffer for 60 min. After an additional wash with sodium cacodylate 0.1 M buffer, the muscle was stained with 1.5% aqueous Uranyl acetate for 60 min. Samples were dehydrated in a graded ethanol series, followed by acetonitrile for 15 min at room temperature. Samples were embedded in Embed 812 resin (Electron Microscopy Sciences, Hatfield, PA). Samples were cut at 55-60 nm (silver-gold) using a Diatome diamond knife (Diatome, USA, Hatfield, PA) on a Leica Ultracut S ultramicrotome. Sections were contrasted with lead citrate and viewed on a JSM 1400 electron microscope (JEOL, USA, Inc., Peabody, MA) operated at 100 kV. Digital images were recorded using a Veleta 2K x2K camera (EMSIS, GmbH).

Lipolysis Assay. The entire gWAT fat depot was isolated, weighed, and cut. 30-50 mg of tissue was incubated in 600 ul per well of filtered lipolysis medium (DMEM, 2% BSA) with or without Isoproterenol (1µM). At various time points during incubation at 37°C, the medium was collected and glycerol concentration was measured using a free glycerol

determination kit (Sigma-Aldrich) according to the manufacturer's instructions. Sample absorbance was measured at 540 nm, using the Epoch™ 2 Microplate Spectrophotometer (BioTek), and glycerol content was normalized to the initial tissue weight.

Muscle enzyme activity. Citrate Synthase (CS) and 6-phosphofructokinase (6-PFK) enzyme activity were quantified from EDL and soleus protein lysate using commercially available colorimetric assay kits (CS0720 Sigma-Aldrich Citrate Synthase; and 6-Phosphofructokinase Activity Assay - ab155898) according to the manufacturer's instructions and quantified using an Epoch™ 2 Microplate Spectrophotometer (BioTek).

Quantification and Statistical Analysis

Statistical Analyses. Data are expressed as mean ± standard error of the mean (SEM). Statistical significance for normally distributed data was determined using Student's t-tests for comparisons of 2 groups or analysis of variance (ANOVA) followed by Fisher LSD post-hoc tests for comparisons of 3 or more groups. For metabolic cage analyses, ANOVA with repeated measures and Fisher LSD post-hoc tests were used. Significance was set at $P<0.05$. Statistical analyses were performed with Prism 7 (GraphPad Software) unless otherwise indicated. Quantification of Western blots was performed using ImageJ 1.53a.

Study Approval.

All animal care and treatments were carried out in compliance with Weill Cornell Medical College Institutional Animal Care and Use Committee guidelines.

Data and Code Availability. All data and code to understand and assess the conclusion of this research are available in the main text, supplementary materials, or GEO Database (accession number TBD).

Resource Availability

Lead Contact

Requests for resources and reagents should be directed to and will be fulfilled by the Lead Contact, Marcus D. Goncalves (mdg9010@med.cornell.edu).

Materials Availability

All reagents are available from the Lead Contact under a material transfer agreement with Weill Cornell Medicine.

Bibliography

1. Peixoto da Silva, S., Santos, J. M. O., Costa E Silva, M. P., Gil da Costa, R. M. & Medeiros, R. Cancer cachexia and its pathophysiology: links with sarcopenia, anorexia and asthenia. *J. Cachexia. Sarcopenia Muscle* **11,** 619–635 (2020).

2. Wang, L., Shao, Y. Y. & Ballock, R. T. Leptin synergizes with thyroid hormone signaling in promoting growth plate chondrocyte proliferation and terminal differentiation in vitro. *Bone* **48,** 1022–1027 (2011).

3. Yavuz, S., Salgado Nunez Del Prado, S. & Celi, F. S. Thyroid hormone action and energy expenditure. *Journal of the Endocrine Society* **3,** 1345–1356 (2019).

4. Chong, P. K., Jung, R. T., Scrimgeour, C. M. & Rennie, M. J. The effect of pharmacological dosages of glucocorticoids on free living total energy expenditure in man. *Clin. Endocrinol. (Oxf.)* **40,** 577–581 (1994).

5. Hills, A. P., Mokhtar, N. & Byrne, N. M. Assessment of physical activity and energy expenditure: an overview of objective measures. *Front. Nutr.* **1,** 5 (2014).

6. Purcell, S. A., Elliott, S. A., Baracos, V. E., Chu, Q. S. C. & Prado, C. M. Key determinants of energy expenditure in cancer and implications for clinical practice. *Eur. J. Clin. Nutr.* **70,** 1230–1238 (2016).

7. Lim, S. *et al.* Cold-induced activation of brown adipose tissue and adipose angiogenesis in mice. *Nat. Protoc.* **7,** 606–615 (2012).

8. Kazak, L. *et al.* A creatine-driven substrate cycle enhances energy expenditure and thermogenesis in beige fat. *Cell* **163,** 643–655 (2015).

9. Petruzzelli, M. *et al.* A switch from white to brown fat increases energy expenditure in cancer-associated cachexia. *Cell Metab.* **20,** 433–447 (2014).

10. Kir, S. & Spiegelman, B. M. Cachexia & brown fat: a burning issue in cancer. *Trends Cancer* **2,** 461–463 (2016).

11. Goncalves, M. D. *et al.* Fenofibrate prevents skeletal muscle loss in mice with lung cancer. *Proc. Natl. Acad. Sci. USA* **115,** E743–E752 (2018).

12. Wang, G. *et al.* Metastatic cancers promote cachexia through ZIP14 upregulation in skeletal muscle. *Nat. Med.* **24,** 770–781 (2018).

13. Perdikari, A. *et al.* BATLAS: deconvoluting brown adipose tissue. *Cell Rep.* **25,** 784–797.e4 (2018).

14. Rosenbaum, M. & Leibel, R. L. Models of energy homeostasis in response to maintenance of reduced body weight. *Obesity (Silver Spring)* **24,** 1620–1629 (2016).

15. Goldsmith, R. *et al.* Effects of experimental weight perturbation on skeletal muscle work efficiency, fuel utilization, and biochemistry in human subjects. *Am. J. Physiol. Regul. Integr. Comp. Physiol.* **298,** R79–88 (2010).

16. Jin, L. *et al.* Phosphorylation-mediated activation of LDHA promotes cancer cell invasion and tumour metastasis. *Oncogene* **36,** 3797–3806 (2017).

17. Pilegaard, H. *et al.* PDH-E1alpha dephosphorylation and activation in human skeletal muscle during exercise: effect of intralipid infusion. *Diabetes* **55,** 3020–3027 (2006).

18. Speakman, J. R. & Mitchell, S. E. Caloric restriction. *Mol. Aspects Med.* **32,** 159–221 (2011).

19. Van Klinken, J. B., van den Berg, S. A. A., Havekes, L. M. & Willems Van Dijk, K. Estimation of activity related energy expenditure and resting metabolic rate in freely moving mice from indirect calorimetry data. *PLoS One* **7,** e36162 (2012).

20. Pons, V. *et al.* Calorie restriction regime enhances physical performance of trained athletes. *J. Int. Soc. Sports Nutr.* **15,** 12 (2018).

21. Redman, L. M. *et al.* Metabolic Slowing and Reduced Oxidative Damage with Sustained Caloric Restriction Support the Rate of Living and Oxidative Damage Theories of Aging. *Cell Metab.* **27,** 805–815.e4 (2018).

22. Suriben, R. *et al.* Antibody-mediated inhibition of GDF15-GFRAL activity reverses cancer cachexia in mice. *Nat. Med.* **26,** 1264–1270 (2020).

23. Puri, P. *et al.* Pediatric positive airway pressure adherence in obstructive sleep apnea enhanced by family member positive airway pressure usage. *J. Clin. Sleep Med.* **12,** 959–963 (2016).

24. Lerner, L. *et al.* MAP3K11/GDF15 axis is a critical driver of cancer cachexia. *J. Cachexia. Sarcopenia Muscle* **7,** 467–482 (2016).

25. Lerner, L. *et al.* Plasma growth differentiation factor 15 is associated with weight loss and mortality in cancer patients. *J. Cachexia. Sarcopenia Muscle* **6,** 317–324 (2015).

26. Johnen, H. *et al.* Tumor-induced anorexia and weight loss are mediated by the TGF-beta superfamily cytokine MIC-1. *Nat. Med.* **13,** 1333–1340 (2007).

27. Chen, J. L. *et al.* Differential Effects of IL6 and Activin A in the Development of Cancer-Associated Cachexia. *Cancer Res.* **76,** 5372–5382 (2016).

28. Fournier, B. *et al.* Blockade of the activin receptor IIb activates functional brown adipogenesis and thermogenesis by inducing mitochondrial oxidative metabolism. *Mol. Cell. Biol.* **32,** 2871–2879 (2012).

29. Wakabayashi, H., Arai, H. & Inui, A. The regulatory approval of anamorelin for treatment of cachexia in patients with non-small cell lung cancer, gastric cancer, pancreatic cancer, and colorectal cancer in Japan: facts and numbers. *J. Cachexia. Sarcopenia Muscle* **12,** 14–16 (2021).

30. Garcia, J. M. & Polvino, W. J. Pharmacodynamic hormonal effects of anamorelin, a novel oral ghrelin mimetic and growth hormone secretagogue in healthy volunteers. *Growth Horm IGF Res* **19,** 267–273 (2009).

31. Hamauchi, S. *et al.* A multicenter, open-label, single-arm study of anamorelin (ONO-7643) in advanced gastrointestinal cancer patients with cancer cachexia. *Cancer* **125,** 4294–4302 (2019).

32. Katakami, N. *et al.* Anamorelin (ONO-7643) for the treatment of patients with non-small cell lung cancer and cachexia: Results from a randomized, double-blind, placebo-controlled, multicenter study of Japanese patients (ONO-7643-04). *Cancer* **124,** 606–616 (2018).

33. Leibel, R. L., Rosenbaum, M. & Hirsch, J. Changes in energy expenditure resulting from altered body weight. *N. Engl. J. Med.* **332,** 621–628 (1995).

34. Bernardo, B. *et al.* Characterization of cachexia in the human fibrosarcoma HT-1080 mouse tumour model. *J. Cachexia. Sarcopenia Muscle* (2020). doi:10.1002/jcsm.12618

35. Rosenbaum, M., Murphy, E. M., Heymsfield, S. B., Matthews, D. E. & Leibel, R. L. Low dose leptin administration reverses effects of sustained weight-reduction on energy expenditure and circulating concentrations of thyroid hormones. *J. Clin. Endocrinol. Metab.* **87,** 2391–2394 (2002).

36. Rosenbaum, M. *et al.* Effects of experimental weight perturbation on skeletal muscle work efficiency in human subjects. *Am. J. Physiol. Regul. Integr. Comp. Physiol.* **285,** R183–92 (2003).

37. Fraga, A. *et al.* Temperature but not leptin prevents semi-starvation induced hyperactivity in rats: implications for anorexia nervosa treatment. *Sci. Rep.* **10,** 5300 (2020).

38. Exner, C. *et al.* Leptin suppresses semi-starvation induced hyperactivity in rats: implications for anorexia nervosa. *Mol. Psychiatry* **5,** 476–481 (2000).

39. Rohm, M. *et al.* An AMP-activated protein kinase-stabilizing peptide ameliorates adipose tissue wasting in cancer cachexia in mice. *Nat. Med.* **22,** 1120–1130 (2016).

40. Das, S. K. *et al.* Adipose triglyceride lipase contributes to cancer-associated cachexia. *Science* **333,** 233–238 (2011).

41. Kir, S. *et al.* Tumour-derived PTH-related protein triggers adipose tissue browning and cancer cachexia. *Nature* **513,** 100–104 (2014).

42. Gibney, E., Elia, M., Jebb, S. A., Murgatroyd, P. & Jennings, G. Total energy expenditure in patients with small-cell lung cancer: results of a validated study using the bicarbonate-urea method. *Metab. Clin. Exp.* **46,** 1412–1417 (1997).

43. Staal-van den Brekel, A. J., Dentener, M. A., Schols, A. M., Buurman, W. A. & Wouters, E. F. Increased resting energy expenditure and weight loss are related to a systemic inflammatory response in lung cancer patients. *J. Clin. Oncol.* **13,** 2600–2605 (1995).

44. Jatoi, A., Daly, B. D., Hughes, V., Dallal, G. E. & Roubenoff, R. The prognostic effect of increased resting energy expenditure prior to treatment for lung cancer. *Lung Cancer* **23,** 153–158 (1999).

45. Nixon, D. W. *et al.* Resting energy expenditure in lung and colon cancer. *Metab. Clin. Exp.* **37,** 1059–1064 (1988).

46. Jatoi, A. *et al.* Do patients with nonmetastatic non-small cell lung cancer demonstrate altered resting energy expenditure? *Ann. Thorac. Surg.* **72,** 348–351 (2001).

47. Richards, E. W. *et al.* Glucose metabolism in advanced lung cancer patients. *Nutrition* **8,** 245–251 (1992).

48. Becker, A. S. *et al.* Brown fat does not cause cachexia in cancer patients: A large retrospective longitudinal FDG-PET/CT cohort study. *PLoS One* **15,** e0239990 (2020).

49. Blum, D. *et al.* Cancer cachexia: a systematic literature review of items and domains associated with involuntary weight loss in cancer. *Crit. Rev. Oncol. Hematol.* **80,** 114–144 (2011).

50. Miranda, C. S. *et al.* PPAR-α activation counters brown adipose tissue whitening: a comparative study between high-fat- and high-fructose-fed mice. *Nutrition* **78,** 110791 (2020).

51. Wang, Q. *et al.* The hepatokine Tsukushi gates energy expenditure via brown fat sympathetic innervation. *Nat. Metab.* **1,** 251–260 (2019).

52. Kamei, Y. *et al.* Skeletal muscle FOXO1 (FKHR) transgenic mice have less skeletal muscle mass, down-regulated Type I (slow twitch/red muscle) fiber genes, and impaired glycemic control. *J. Biol. Chem.* **279,** 41114–41123 (2004).

53. Goncalves, M. D. *et al.* Akt deficiency attenuates muscle size and function but not the response to ActRIIB inhibition. *PLoS One* **5,** e12707 (2010).

54. Lerner, L. *et al.* Growth differentiating factor-15 (GDF-15): A potential biomarker and therapeutic target for cancer-associated weight loss. *Oncol. Lett.* **12,** 4219–4223 (2016).

55. Loumaye, A. *et al.* Role of Activin A and myostatin in human cancer cachexia. *J. Clin. Endocrinol. Metab.* **100,** 2030–2038 (2015).

56. Loumaye, A. *et al.* Circulating Activin A predicts survival in cancer patients. *J. Cachexia. Sarcopenia Muscle* **8,** 768–777 (2017).

57. Hoda, M. A. *et al.* High circulating activin A level is associated with tumor progression and predicts poor prognosis in lung adenocarcinoma. *Oncotarget* **7,** 13388–13399 (2016).

58. Zhou, X. *et al.* Reversal of cancer cachexia and muscle wasting by ActRIIB antagonism leads to prolonged survival. *Cell* **142,** 531–543 (2010).

59. Busquets, S. *et al.* Myostatin blockage using actRIIB antagonism in mice bearing the Lewis lung carcinoma results in the improvement of muscle wasting and physical performance. *J. Cachexia. Sarcopenia Muscle* **3,** 37–43 (2012).

60. Jones, J. E. *et al.* Supraphysiologic administration of GDF11 induces cachexia in part by upregulating GDF15. *Cell Rep.* **22,** 1522–1530 (2018).

61. Richer, A. L. *et al.* WEE1 Kinase Inhibitor AZD1775 Has Preclinical Efficacy in LKB1-Deficient Non-Small Cell Lung Cancer. *Cancer Res.* **77,** 4663–4672 (2017).

62. Zhang, M. *et al.* CCL7 recruits cDC1 to promote antitumor immunity and facilitate checkpoint immunotherapy to non-small cell lung cancer. *Nat. Commun.* **11,** 6119 (2020).

63. Zhong, X. & Zimmers, T. A. Sex differences in cancer cachexia. *Curr. Osteoporos. Rep.* **18,** 646–654 (2020).

64. Lovejoy, J. C., Sainsbury, A. & Stock Conference 2008 Working Group. Sex differences in obesity and the regulation of energy homeostasis. *Obes. Rev.* **10,** 154–167 (2009).

65. Cosper, P. F. & Leinwand, L. A. Cancer causes cardiac atrophy and autophagy in a sexually dimorphic manner. *Cancer Res.* **71,** 1710–1720 (2011).

66. Palus, S., Akashi, Y., von Haehling, S., Anker, S. D. & Springer, J. The influence of age and sex on disease development in a novel animal model of cardiac cachexia. *Int. J. Cardiol.* **133,** 388–393 (2009).

67. Rosa-Caldwell, M. E. *et al.* Female mice may have exacerbated catabolic signalling response compared to male mice during development and progression of disuse atrophy. *J. Cachexia. Sarcopenia Muscle* (2021). doi:10.1002/jcsm.12693

68. Rooks, D. *et al.* Bimagrumab vs Optimized Standard of Care for Treatment of Sarcopenia in Community-Dwelling Older Adults: A Randomized Clinical Trial. *JAMA Netw. Open* **3,** e2020836 (2020).

69. Ji, H. *et al.* LKB1 modulates lung cancer differentiation and metastasis. *Nature* **448,** 807–810 (2007).

70. Sako, D. *et al.* Characterization of the ligand binding functionality of the extracellular domain of activin receptor type IIb. *J. Biol. Chem.* **285,** 21037–21048 (2010).

71. Breen, D. M. *et al.* GDF-15 Neutralization Alleviates Platinum-Based Chemotherapy-Induced Emesis, Anorexia, and Weight Loss in Mice and Nonhuman Primates. *Cell Metab.* **32,** 938–950.e6 (2020).

72. Pocock, S. J. *Clinical trials: a practical approach*. (books.google.com, 2013).

73. Anton, A. H. & Sayre, D. F. A study of the factors affecting the aluminum oxide-trihydroxyindole procedure for the analysis of catecholamines. *J. Pharmacol. Exp. Ther.* **138,** 360–375 (1962).

74. Goldstein, D. S., Feuerstein, G., Izzo, J. L., Kopin, I. J. & Keiser, H. R. Validity and reliability of liquid chromatography with electrochemical detection for measuring plasma levels of norepinephrine and epinephrine in man. *Life Sci.* **28,** 467–475 (1981).

75. Yuan, M., Breitkopf, S. B., Yang, X. & Asara, J. M. A positive/negative ion-switching, targeted mass spectrometry-based metabolomics platform for bodily fluids, cells, and fresh and fixed tissue. *Nat. Protoc.* **7,** 872–881 (2012).

76. Engström, P. G. *et al.* Systematic evaluation of spliced alignment programs for RNA-seq data. *Nat. Methods* **10,** 1185–1191 (2013).

77. Teng, M. *et al.* A benchmark for RNA-seq quantification pipelines. *Genome Biol.* **17,** 74 (2016).

78. Kucukural, A., Yukselen, O., Ozata, D. M., Moore, M. J. & Garber, M. DEBrowser: interactive differential expression analysis and visualization tool for count data. *BMC Genomics* **20,** 6 (2019).

79. Johnson, W. E., Li, C. & Rabinovic, A. Adjusting batch effects in microarray expression data using empirical Bayes methods. *Biostatistics* **8,** 118–127 (2007).

80. Yu, G., Wang, L.-G., Han, Y. & He, Q.-Y. clusterProfiler: an R package for comparing biological themes among gene clusters. *OMICS* **16,** 284–287 (2012).

81. Axelrod, C. L. *et al.* BAM15-mediated mitochondrial uncoupling protects against obesity and improves glycemic control. *EMBO Mol. Med.* **12,** e12088 (2020).

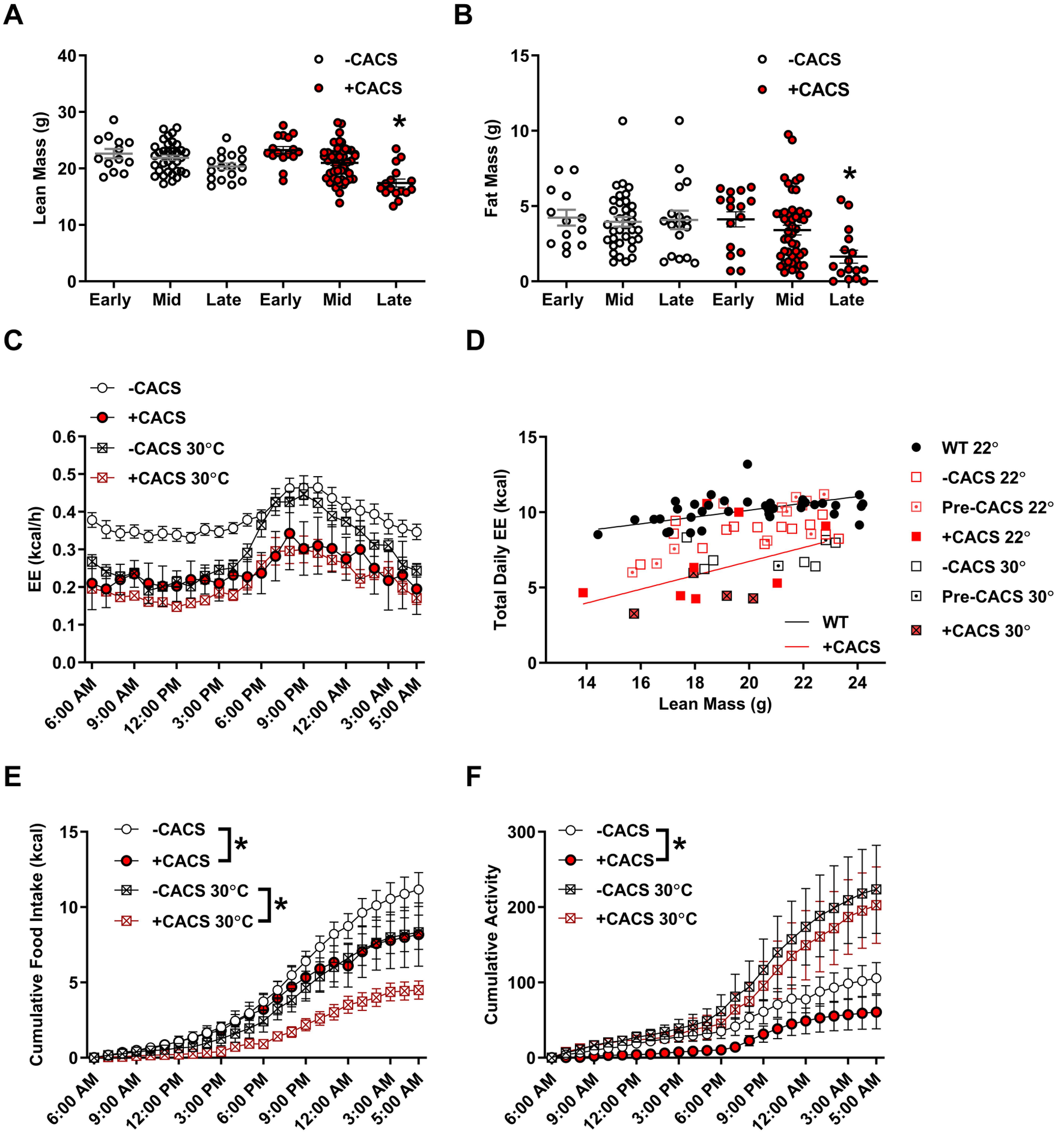
A
Lean Mass (g)
-CACS
+CACS
Early
Mid
Late
B
Fat Mass (g)
C
EE (kcal/h)
-CACS
+CACS
-CACS 30°C
+CACS 30°C
6:00 AM
9:00 AM
12:00 PM
3:00 PM
6:00 PM
9:00 PM
12:00 AM
3:00 AM
5:00 AM
D
Total Daily EE (kcal)
Lean Mass (g)
WT
+CACS
WT 22°
-CACS 22°
Pre-CACS 22°
+CACS 22°
-CACS 30°
Pre-CACS 30°
+CACS 30°
E
Cumulative Food Intake (kcal)
F
Cumulative Activity

Figure 1

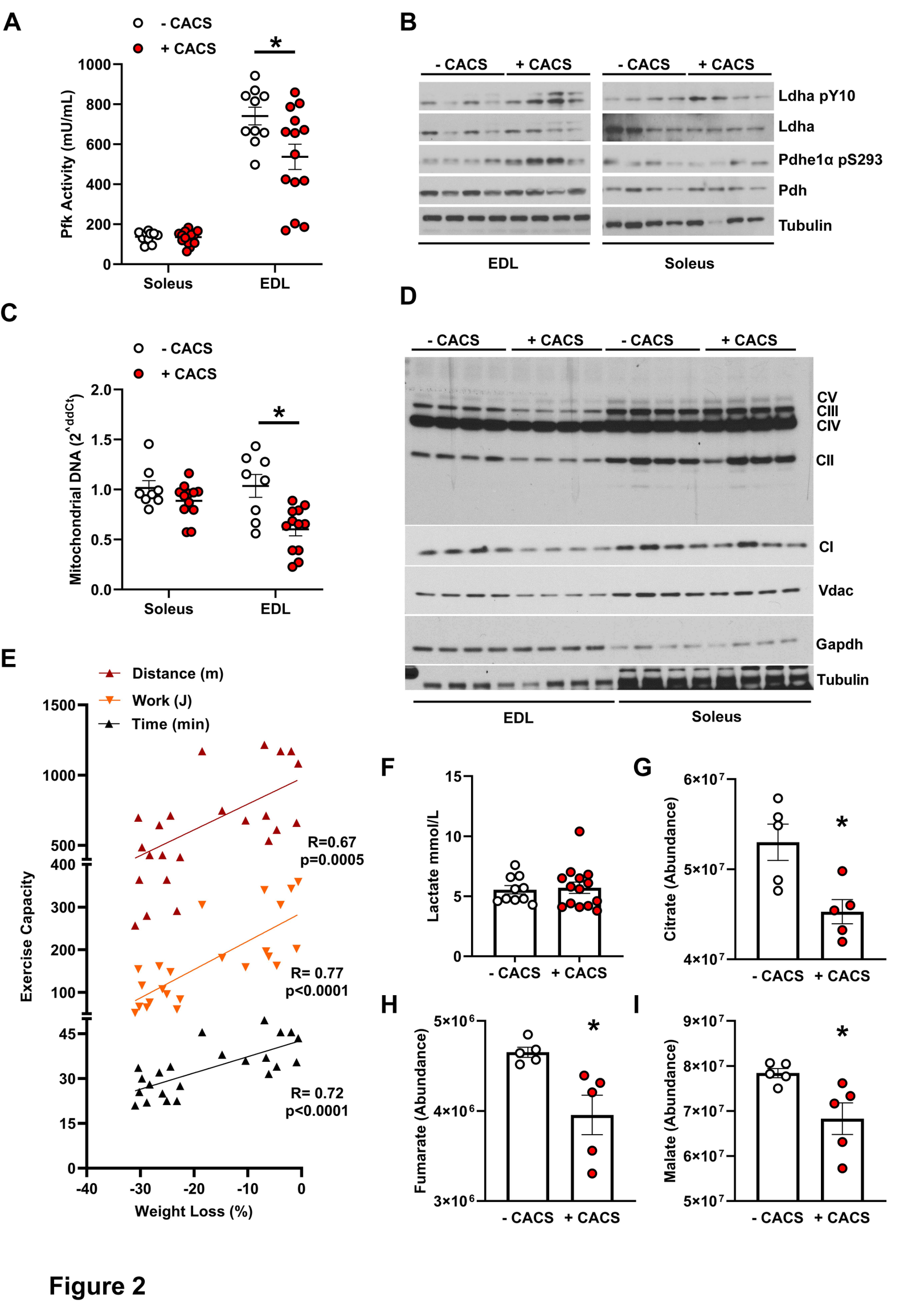
A
- CACS
+ CACS
*
Pfk Activity (mU/mL)
1000
800
600
400
200
0
Soleus
EDL
B
- CACS
+ CACS
- CACS
+ CACS
Ldha pY10
Ldha
Pdhe1α pS293
Pdh
Tubulin
EDL
Soleus
C
- CACS
+ CACS
*
Mitochondrial DNA (2^ddCt)
2.0
1.5
1.0
0.5
0.0
Soleus
EDL
D
- CACS
+ CACS
- CACS
+ CACS
CV
CIII
CIV
CII
CI
Vdac
Gapdh
Tubulin
EDL
Soleus
E
Distance (m)
Work (J)
Time (min)
Exercise Capacity
1500
1000
500
400
300
200
100
45
30
15
0
R=0.67
p=0.0005
R= 0.77
p<0.0001
R= 0.72
p<0.0001
-40
-30
-20
-10
0
Weight Loss (%)
F
Lactate mmol/L
15
10
5
0
- CACS
+ CACS
G
Citrate (Abundance)
6×10^7
5×10^7
4×10^7
*
- CACS
+ CACS
H
Fumarate (Abundance)
5×10^6
4×10^6
3×10^6
*
- CACS
+ CACS
I
Malate (Abundance)
9×10^7
8×10^7
7×10^7
6×10^7
5×10^7
*
- CACS
+ CACS

Figure 2

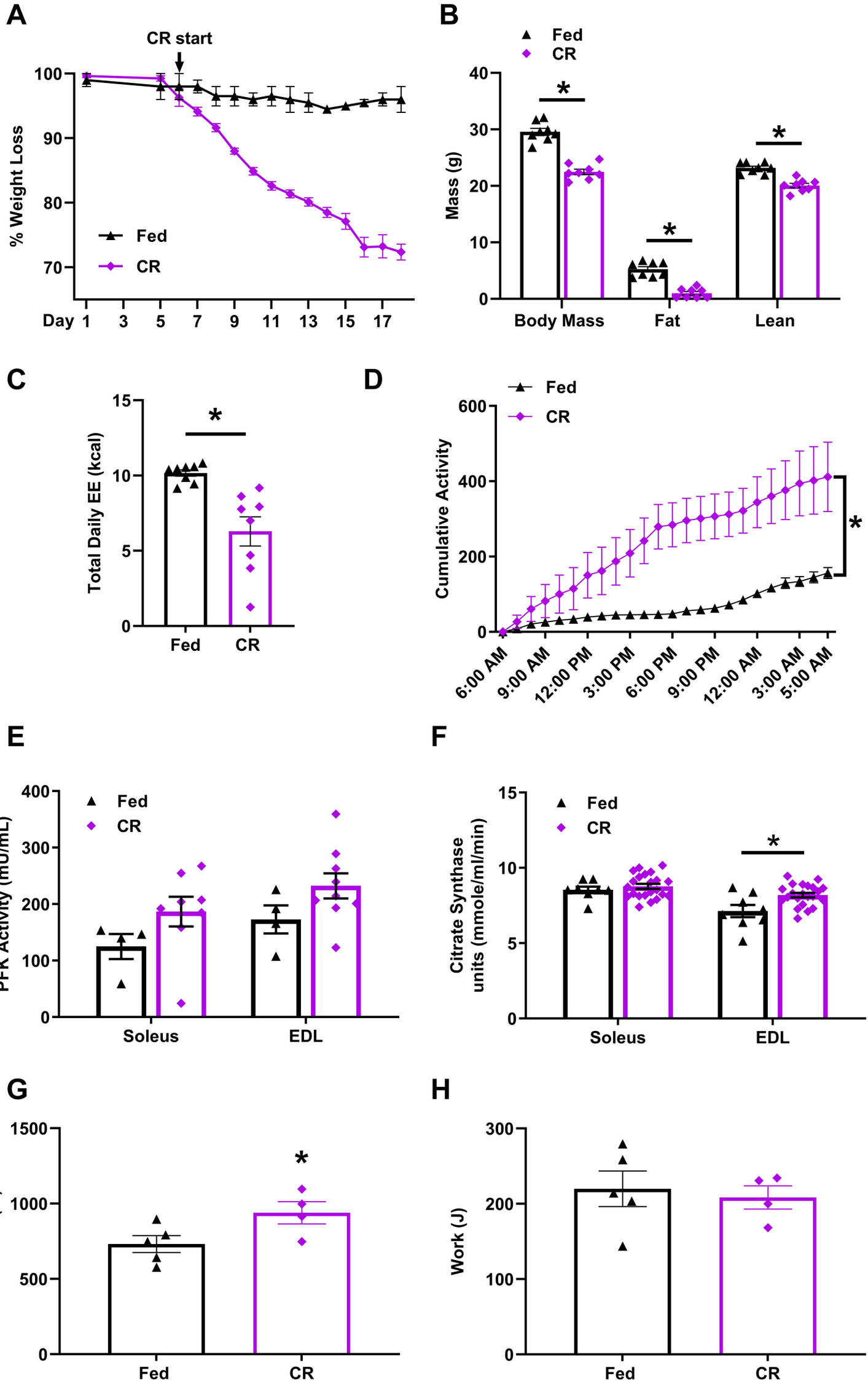
A
CR start
100
90
80
70
% Weight Loss
Fed
CR
Day 1 3 5 7 9 11 13 15 17
B
Fed
CR
40
30
20
10
0
Mass (g)
*
*
*
Body Mass
Fat
Lean
C
15
10
5
0
Total Daily EE (kcal)
*
Fed
CR
D
Fed
CR
600
400
200
0
Cumulative Activity
*
6:00 AM
9:00 AM
12:00 PM
3:00 PM
6:00 PM
9:00 PM
12:00 AM
3:00 AM
5:00 AM
E
400
300
200
100
0
PFK Activity (mU/mL)
Fed
CR
Soleus
EDL
F
15
10
5
0
Citrate Synthase units (mmole/ml/min)
Fed
CR
*
Soleus
EDL
G
1500
1000
500
0
Distance (m)
*
Fed
CR
H
300
200
100
0
Work (J)
Fed
CR

Figure 3

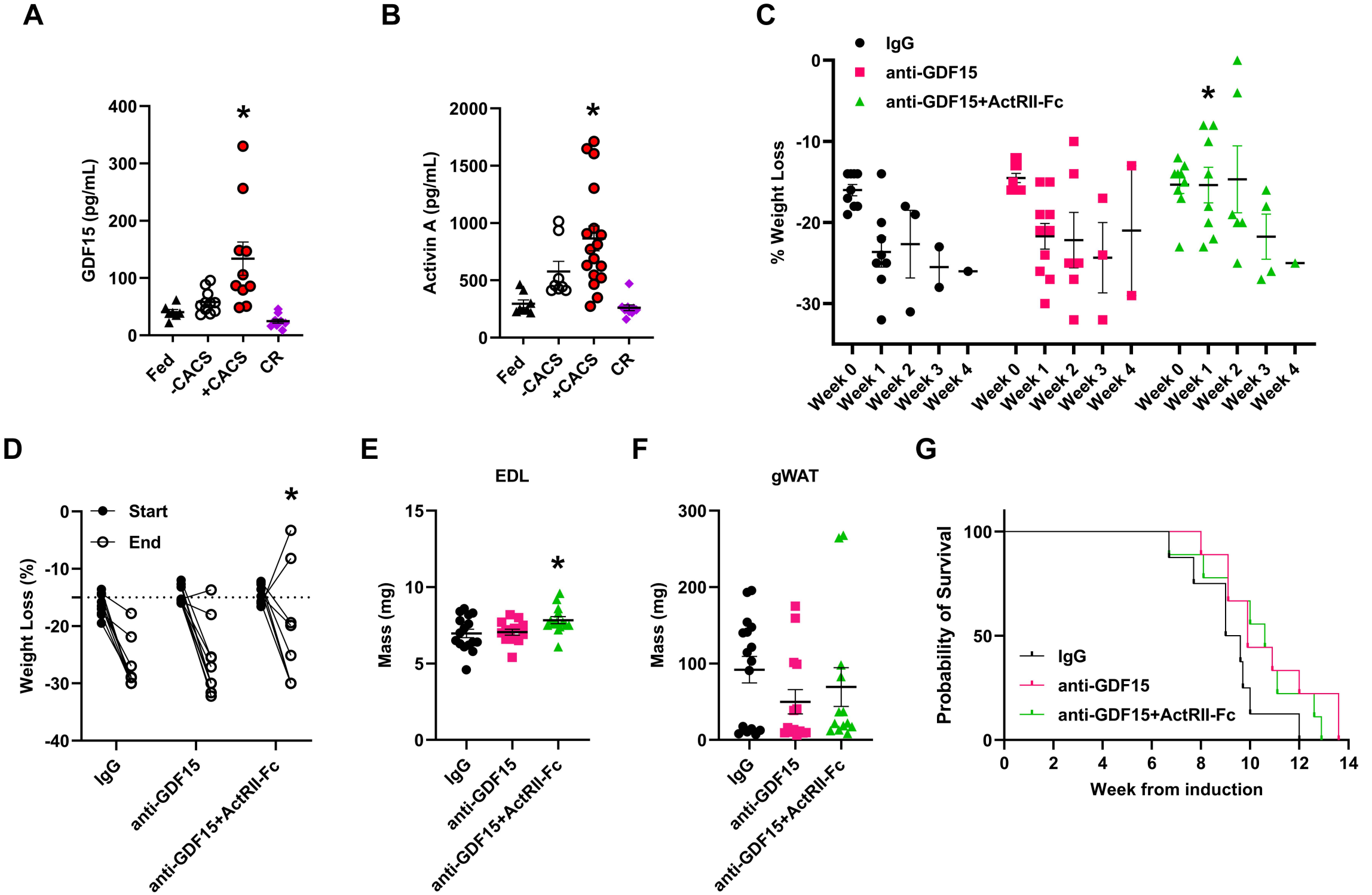
A
GDF15 (pg/mL)
400
300
200
100
0
*
Fed
-CACS
+CACS
CR
B
Activin A (pg/mL)
2000
1500
1000
500
0
*
Fed
-CACS
+CACS
CR
C
IgG
anti-GDF15
anti-GDF15+ActRII-Fc
% Weight Loss
0
-10
-20
-30
*
Week 0
Week 1
Week 2
Week 3
Week 4
D
Start
End
Weight Loss (%)
0
-10
-20
-30
-40
*
IgG
anti-GDF15
anti-GDF15+ActRII-Fc
E
EDL
Mass (mg)
15
10
5
0
*
IgG
anti-GDF15
anti-GDF15+ActRII-Fc
F
gWAT
Mass (mg)
300
200
100
0
IgG
anti-GDF15
anti-GDF15+ActRII-Fc
G
Probability of Survival
100
50
0
IgG
anti-GDF15
anti-GDF15+ActRII-Fc
0
2
4
6
8
10
12
14
Week from induction
H
EE (kcal/h)
0.5
0.4
0.3
0.2
0.1
0.0
IgG
anti-GDF15
anti-GDF15+ActRII-Fc
6:00 AM
9:00 AM
12:00 PM
3:00 PM
6:00 PM
9:00 PM
12:00 AM
3:00 AM
5:00 AM
I
Cumulative Activity (distance)
200
150
100
50
0
IgG
anti-GDF15
anti-GDF15+ActRII-Fc
6:00 AM
9:00 AM
12:00 PM
3:00 PM
6:00 PM
9:00 PM
12:00 AM
3:00 AM
5:00 AM

Figure 4

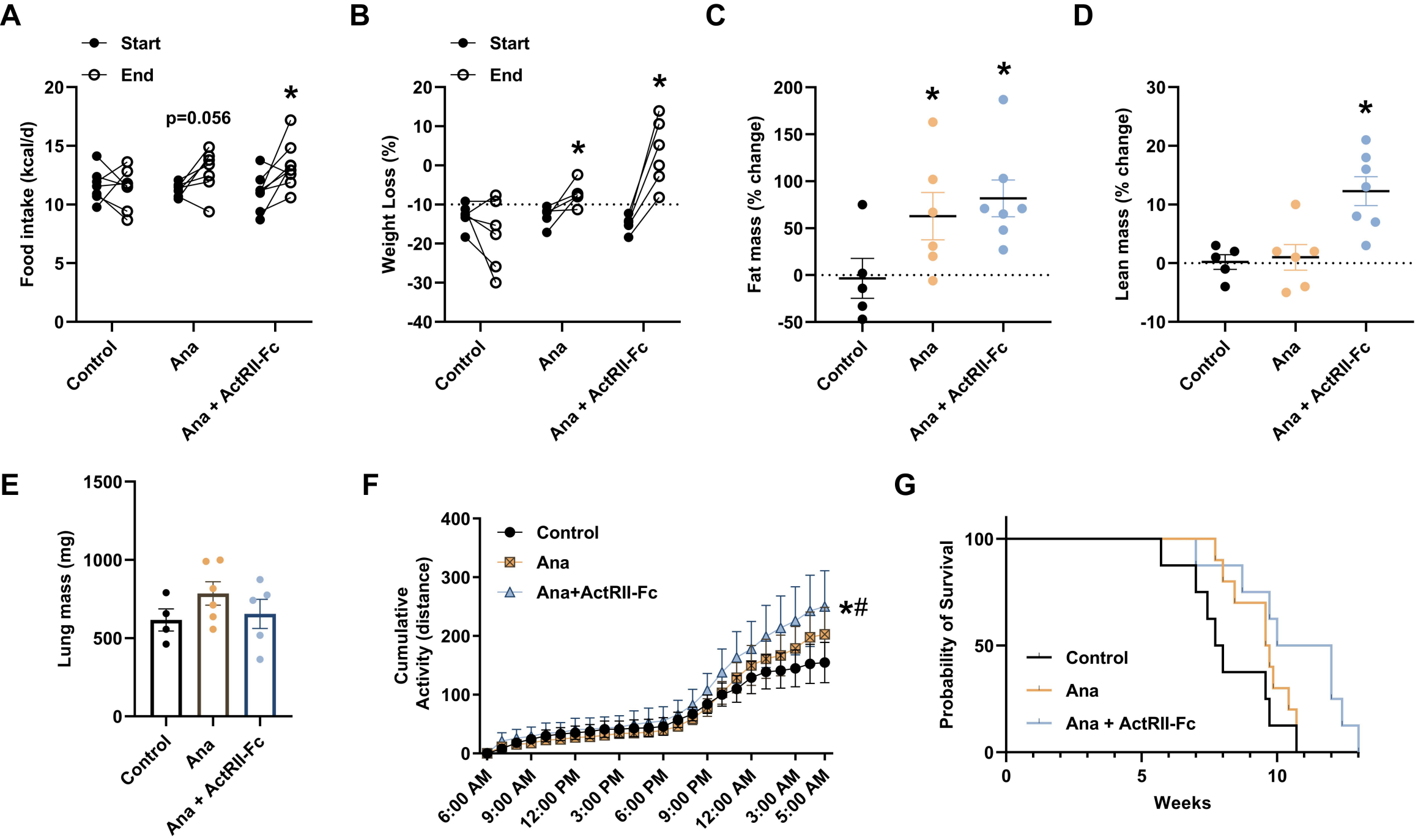
A
Start
End
Food intake (kcal/d)
p=0.056
*
Control
Ana
Ana + ActRII-Fc
B
Start
End
Weight Loss (%)
*
*
Control
Ana
Ana + ActRII-Fc
C
Fat mass (% change)
*
*
Control
Ana
Ana + ActRII-Fc
D
Lean mass (% change)
*
Control
Ana
Ana + ActRII-Fc
E
Lung mass (mg)
Control
Ana
Ana + ActRII-Fc
F
Control
Ana
Ana+ActRII-Fc
Cumulative Activity (distance)
*#
6:00 AM
9:00 AM
12:00 PM
3:00 PM
6:00 PM
9:00 PM
12:00 AM
3:00 AM
5:00 AM
G
Probability of Survival
Control
Ana
Ana + ActRII-Fc
Weeks

Figure 5

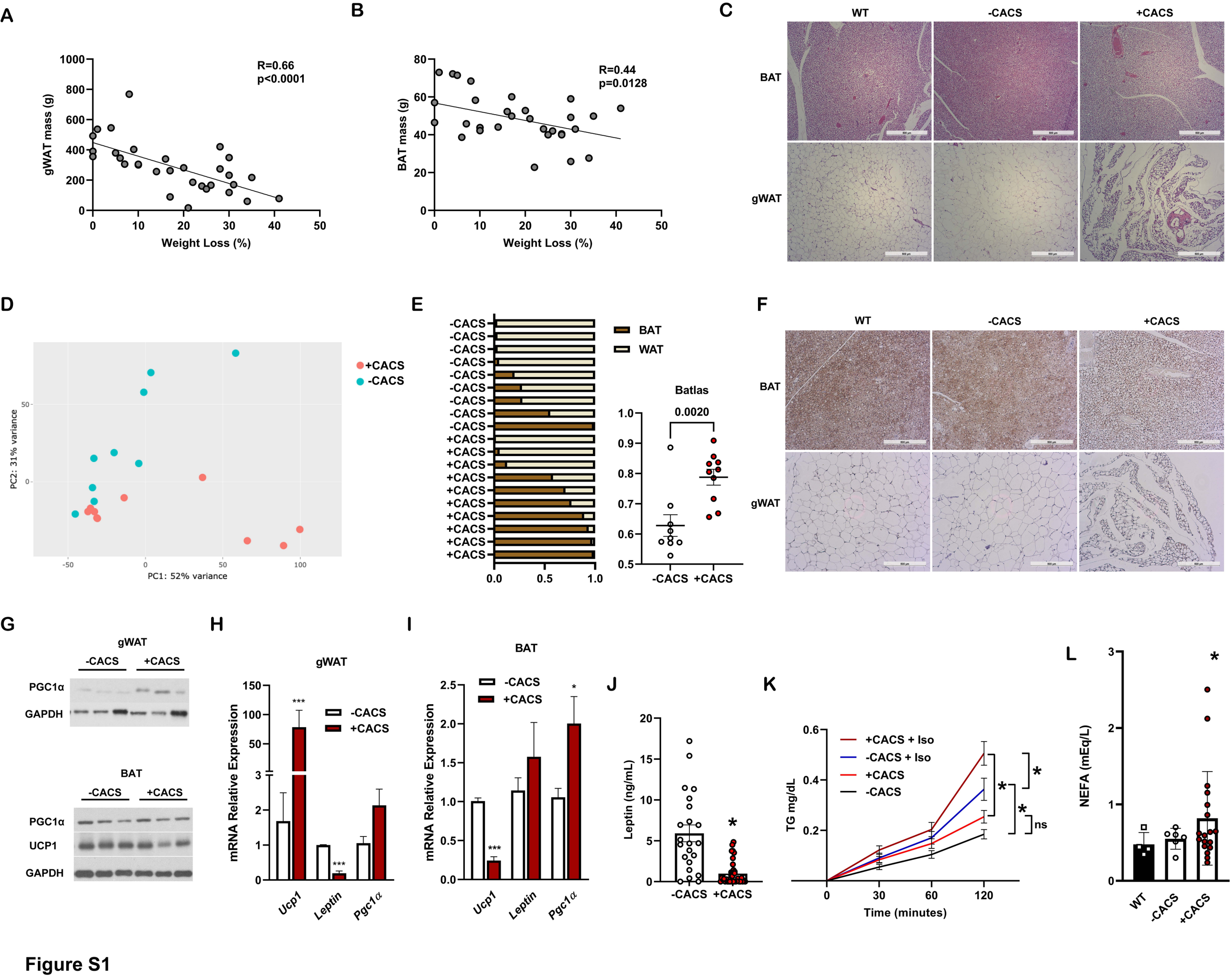
A
gWAT mass (g)
Weight Loss (%)
R=0.66
p<0.0001
B
BAT mass (g)
Weight Loss (%)
R=0.44
p=0.0128
C
WT
-CACS
+CACS
BAT
gWAT
D
+CACS
-CACS
PC2: 31% variance
PC1: 52% variance
E
BAT
WAT
Batlas
0.0020
-CACS
+CACS
F
WT
-CACS
+CACS
BAT
gWAT
G
gWAT
-CACS
+CACS
PGC1α
GAPDH
BAT
-CACS
+CACS
PGC1α
UCP1
GAPDH
H
gWAT
mRNA Relative Expression
-CACS
+CACS
Ucp1
Leptin
Pgc1α
I
BAT
mRNA Relative Expression
-CACS
+CACS
Ucp1
Leptin
Pgc1α
J
Leptin (ng/mL)
-CACS
+CACS
K
+CACS + Iso
-CACS + Iso
+CACS
-CACS
TG mg/dL
Time (minutes)
ns
L
NEFA (mEq/L)
WT
-CACS
+CACS

Figure S1

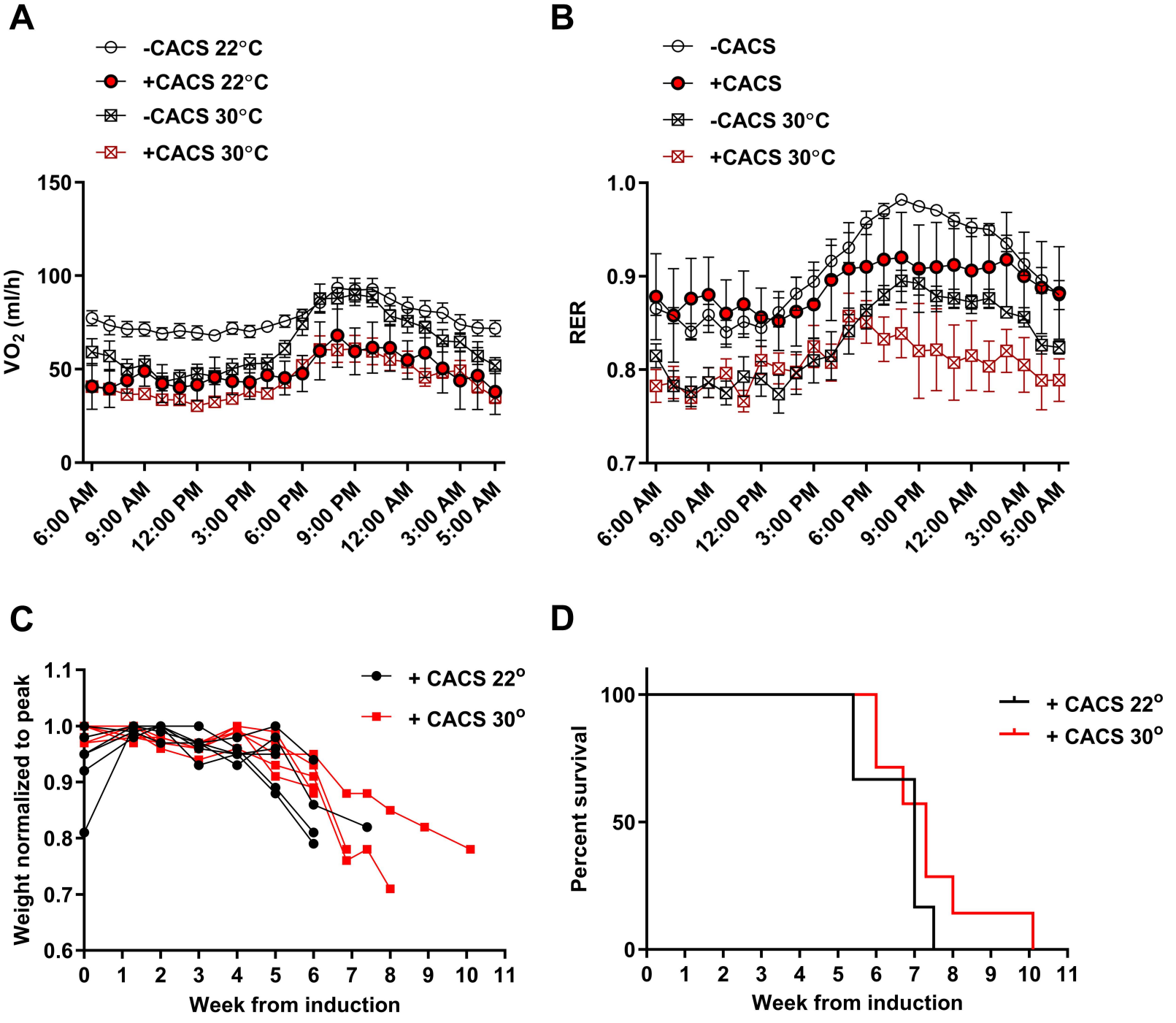
A
-CACS 22°C
+CACS 22°C
-CACS 30°C
+CACS 30°C
VO2 (ml/h)
150
100
50
0
6:00 AM
9:00 AM
12:00 PM
3:00 PM
6:00 PM
9:00 PM
12:00 AM
3:00 AM
5:00 AM
B
-CACS
+CACS
-CACS 30°C
+CACS 30°C
RER
1.0
0.9
0.8
0.7
C
+ CACS 22°
+ CACS 30°
Weight normalized to peak
1.1
1.0
0.9
0.8
0.7
0.6
0 1 2 3 4 5 6 7 8 9 10 11
Week from induction
D
+ CACS 22°
+ CACS 30°
Percent survival
100
50
0
0 1 2 3 4 5 6 7 8 9 10 11
Week from induction

Figure S2

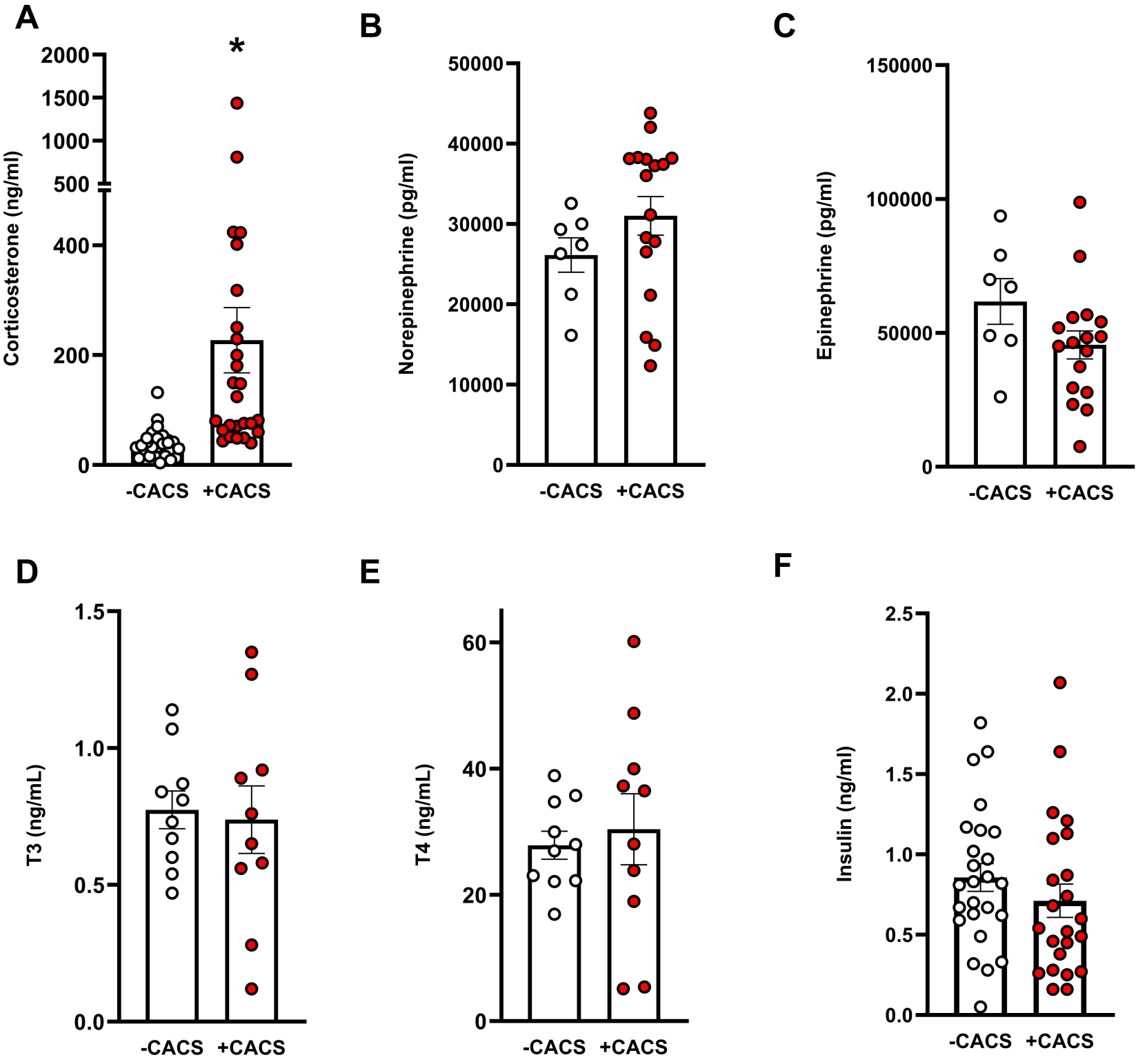
A
Corticosterone (ng/ml)
2000
1500
1000
500
400
200
0
*
-CACS
+CACS
B
Norepinephrine (pg/ml)
50000
40000
30000
20000
10000
0
-CACS
+CACS
C
Epinephrine (pg/ml)
150000
100000
50000
0
-CACS
+CACS
D
T3 (ng/mL)
1.5
1.0
0.5
0.0
-CACS
+CACS
E
T4 (ng/mL)
60
40
20
0
-CACS
+CACS
F
Insulin (ng/ml)
2.5
2.0
1.5
1.0
0.5
0.0
-CACS
+CACS

Figure S3

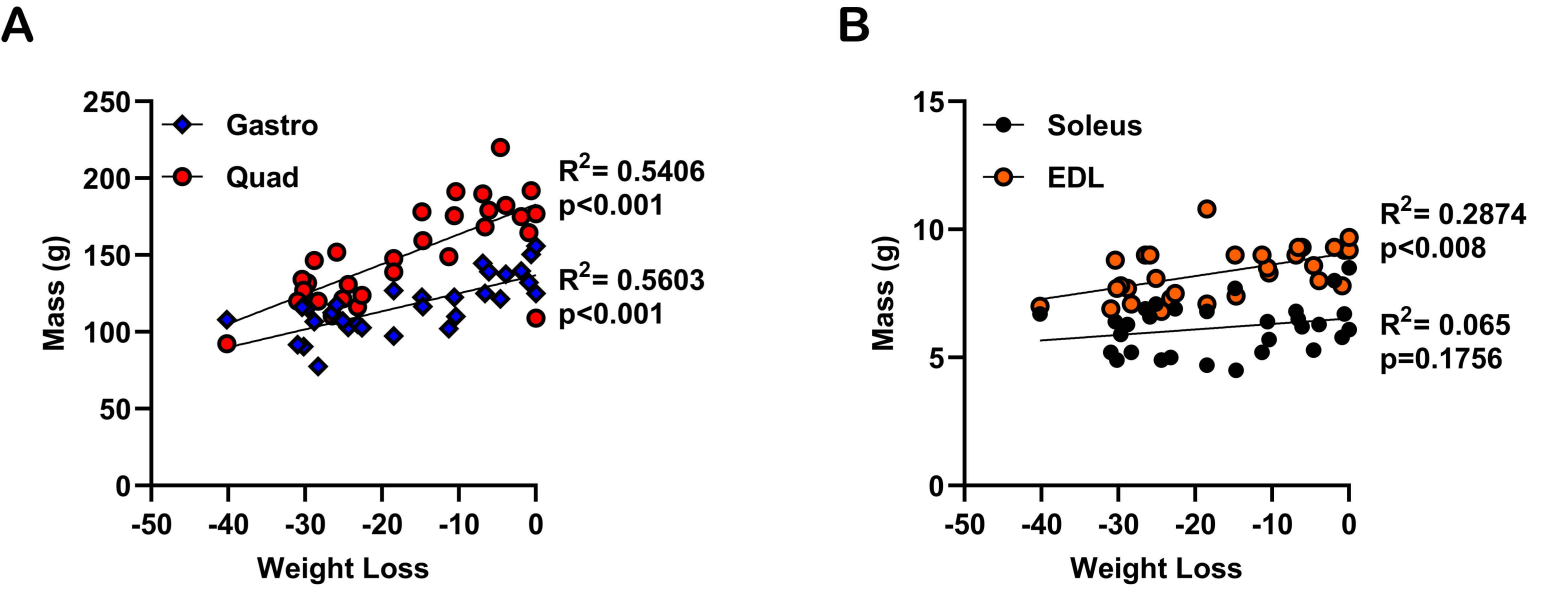
A
250
200
150
100
50
0
Mass (g)
Gastro
Quad
R2= 0.5406
p<0.001
R2= 0.5603
p<0.001
-50
-40
-30
-20
-10
0
Weight Loss
B
15
10
5
0
Mass (g)
Soleus
EDL
R2= 0.2874
p<0.008
R2= 0.065
p=0.1756
-50
-40
-30
-20
-10
0
Weight Loss

Figure S4

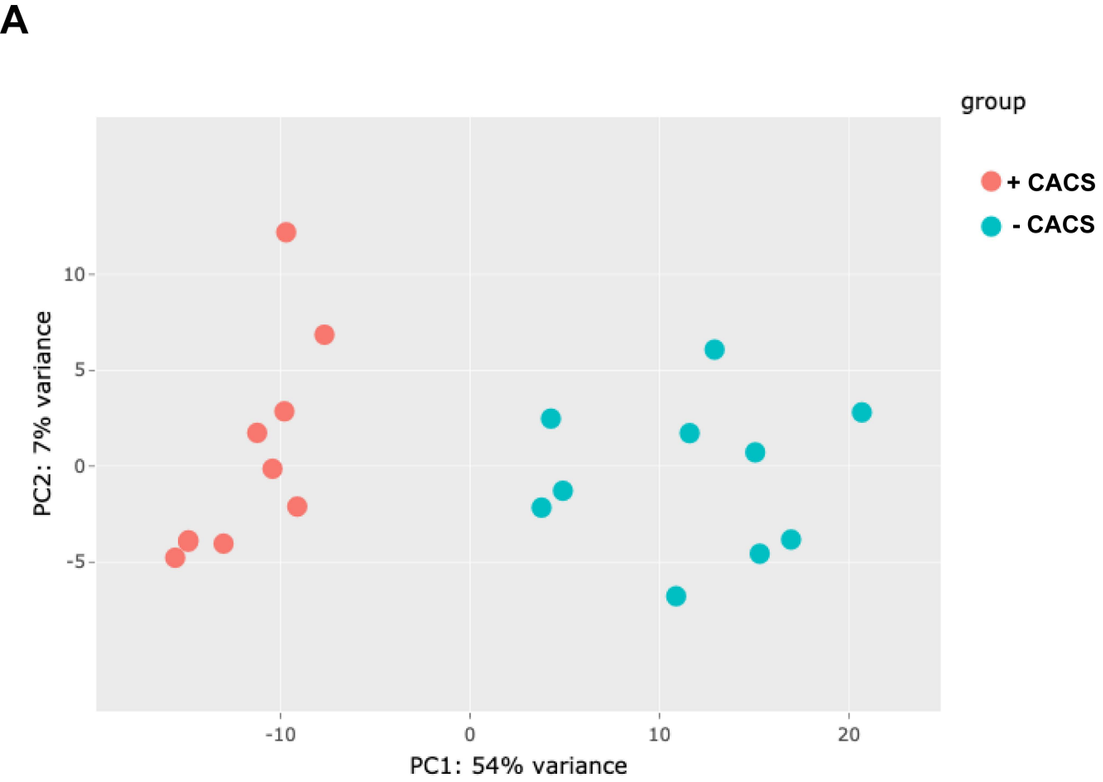
A
group
+ CACS
- CACS
PC2: 7% variance
PC1: 54% variance
10
5
0
-5
-10
0
10
20

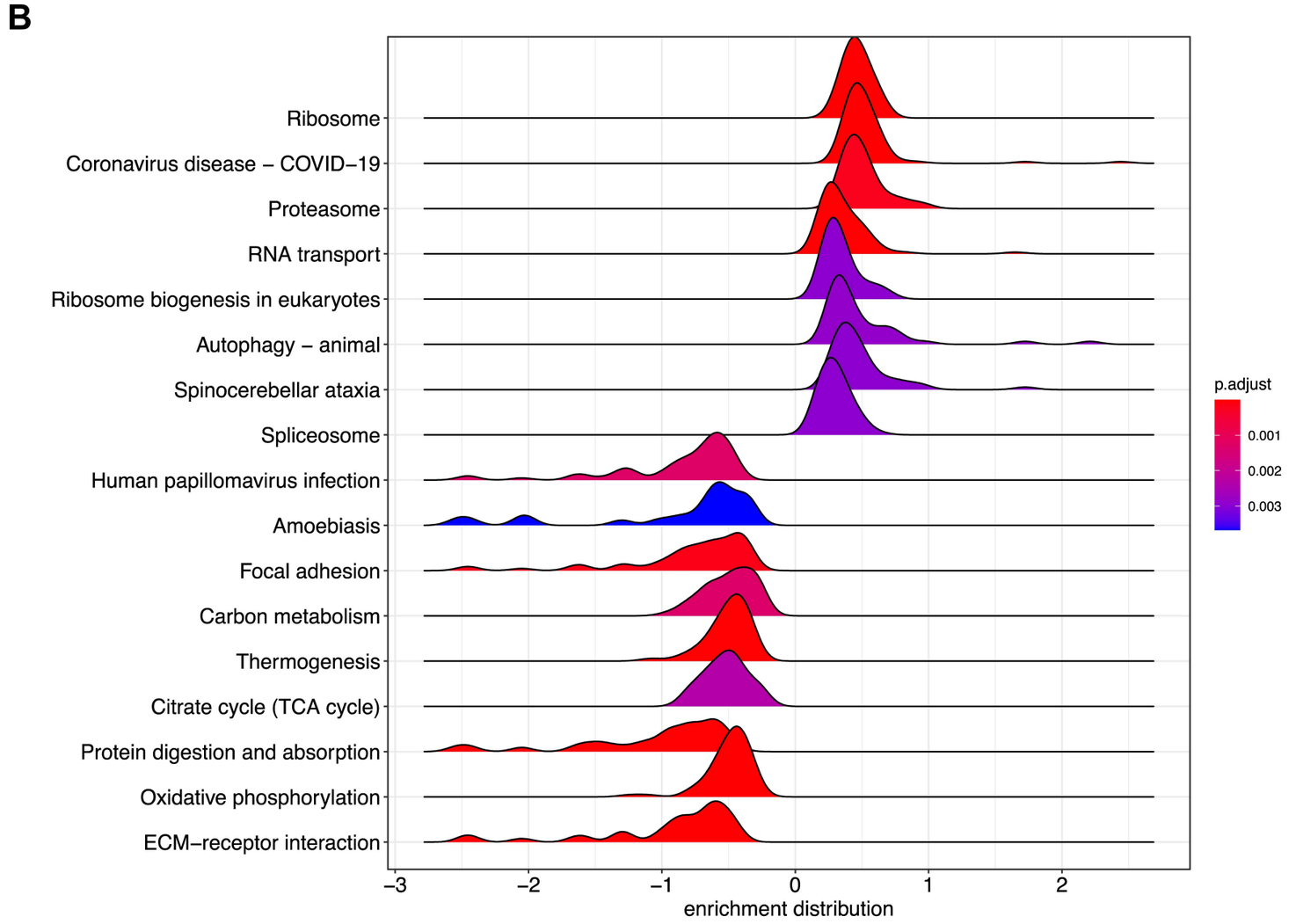
B
Ribosome
Coronavirus disease – COVID–19
Proteasome
RNA transport
Ribosome biogenesis in eukaryotes
Autophagy – animal
Spinocerebellar ataxia
Spliceosome
Human papillomavirus infection
Amoebiasis
Focal adhesion
Carbon metabolism
Thermogenesis
Citrate cycle (TCA cycle)
Protein digestion and absorption
Oxidative phosphorylation
ECM–receptor interaction
p.adjust
0.001
0.002
0.003
−3
−2
−1
0
1
2
enrichment distribution

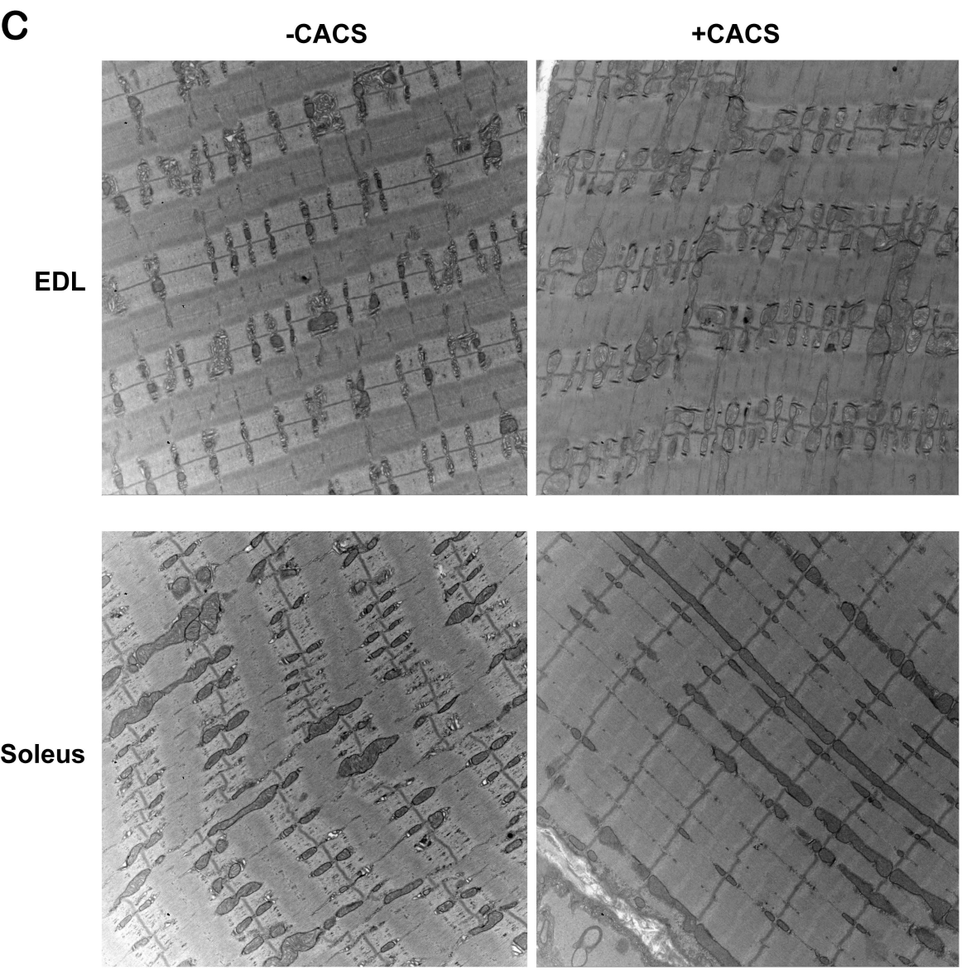
C
-CACS
+CACS
EDL
Soleus

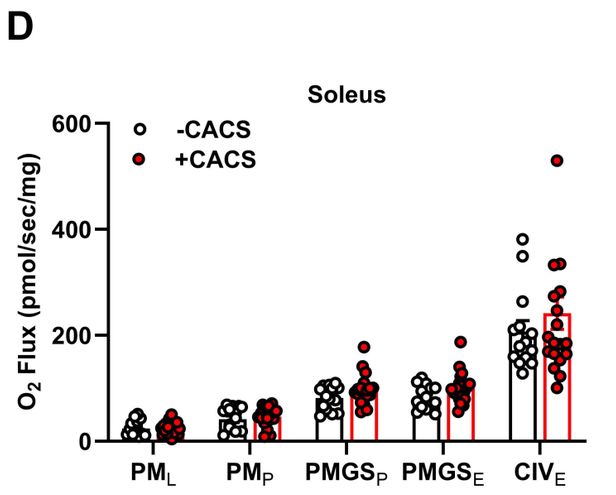
D
Soleus
-CACS
+CACS
O2 Flux (pmol/sec/mg)
600
400
200
0
PML
PMP
PMGSP
PMGSE
CIVE

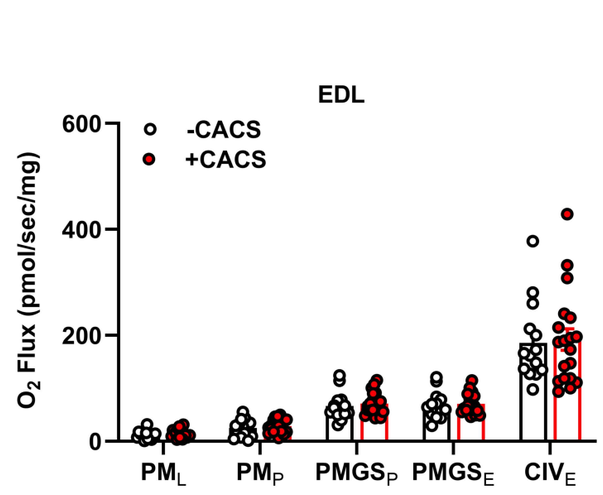
E
EDL
-CACS
+CACS
O2 Flux (pmol/sec/mg)
600
400
200
0
PML
PMP
PMGSP
PMGSE
CIVE

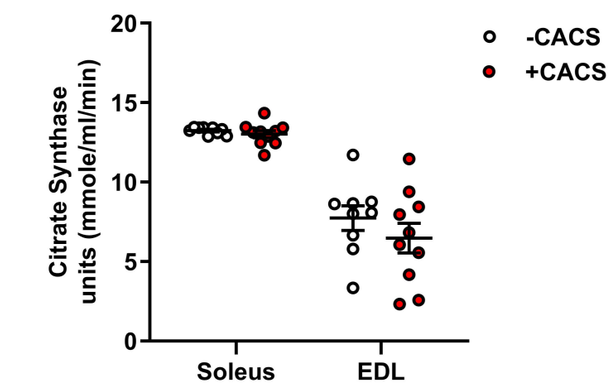
F
-CACS
+CACS
Citrate Synthase units (mmole/ml/min)
20
15
10
5
0
Soleus
EDL

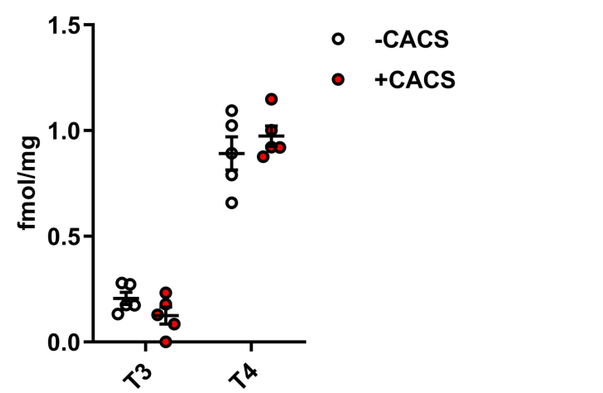
G
-CACS
+CACS
fmol/mg
1.5
1.0
0.5
0.0
T3
T4

Figure S5

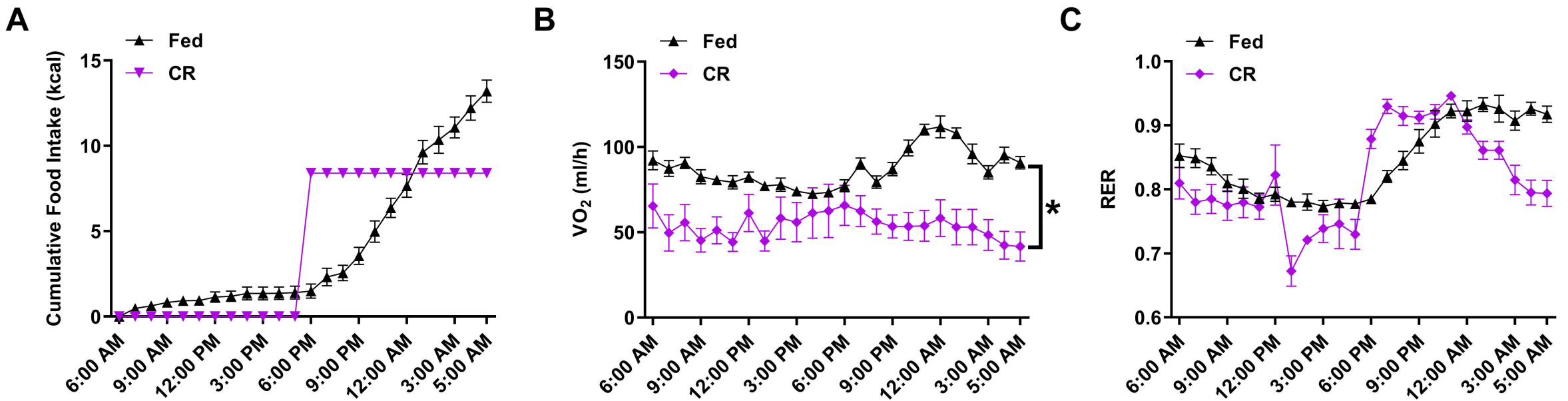
A
Fed
CR
Cumulative Food Intake (kcal)
15
10
5
0
6:00 AM
9:00 AM
12:00 PM
3:00 PM
6:00 PM
9:00 PM
12:00 AM
3:00 AM
5:00 AM
B
Fed
CR
VO2 (ml/h)
150
100
50
0
*
C
Fed
CR
RER
1.0
0.9
0.8
0.7
0.6

Figure S6

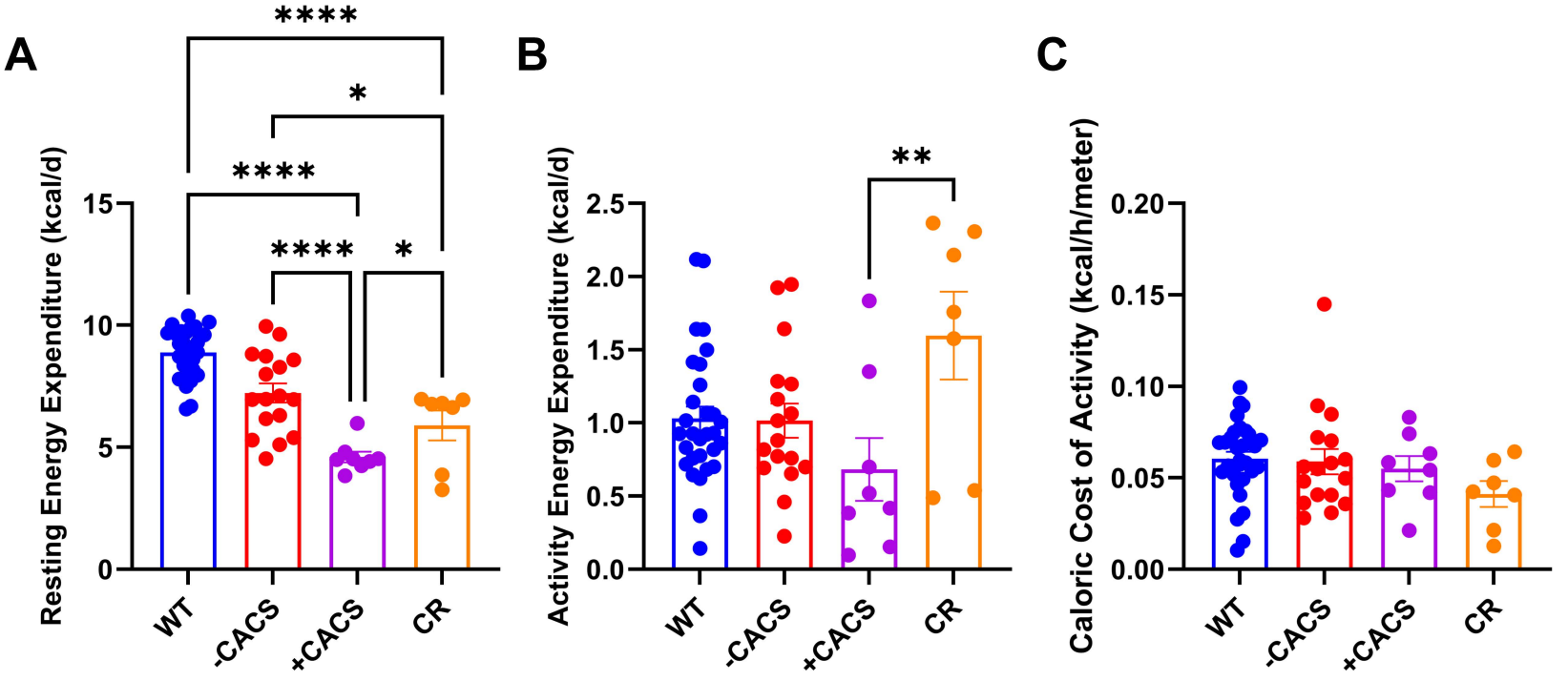
A
B
C
****
*
****
****
*
*
**
Resting Energy Expenditure (kcal/d)
Activity Energy Expenditure (kcal/d)
Caloric Cost of Activity (kcal/h/meter)
0
5
10
15
0.0
0.5
1.0
1.5
2.0
2.5
0.00
0.05
0.10
0.15
0.20
WT
-CACS
+CACS
CR

Figure S7

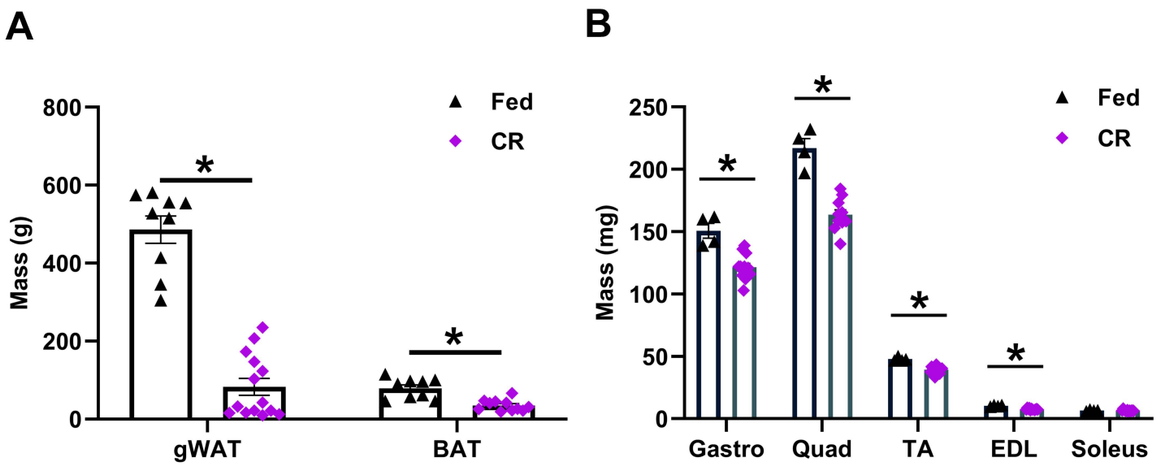
A
Mass (g)
800
600
400
200
0
Fed
CR
*
*
gWAT
BAT

B
Mass (mg)
250
200
150
100
50
0
Fed
CR
*
*
*
*
Gastro
Quad
TA
EDL
Soleus

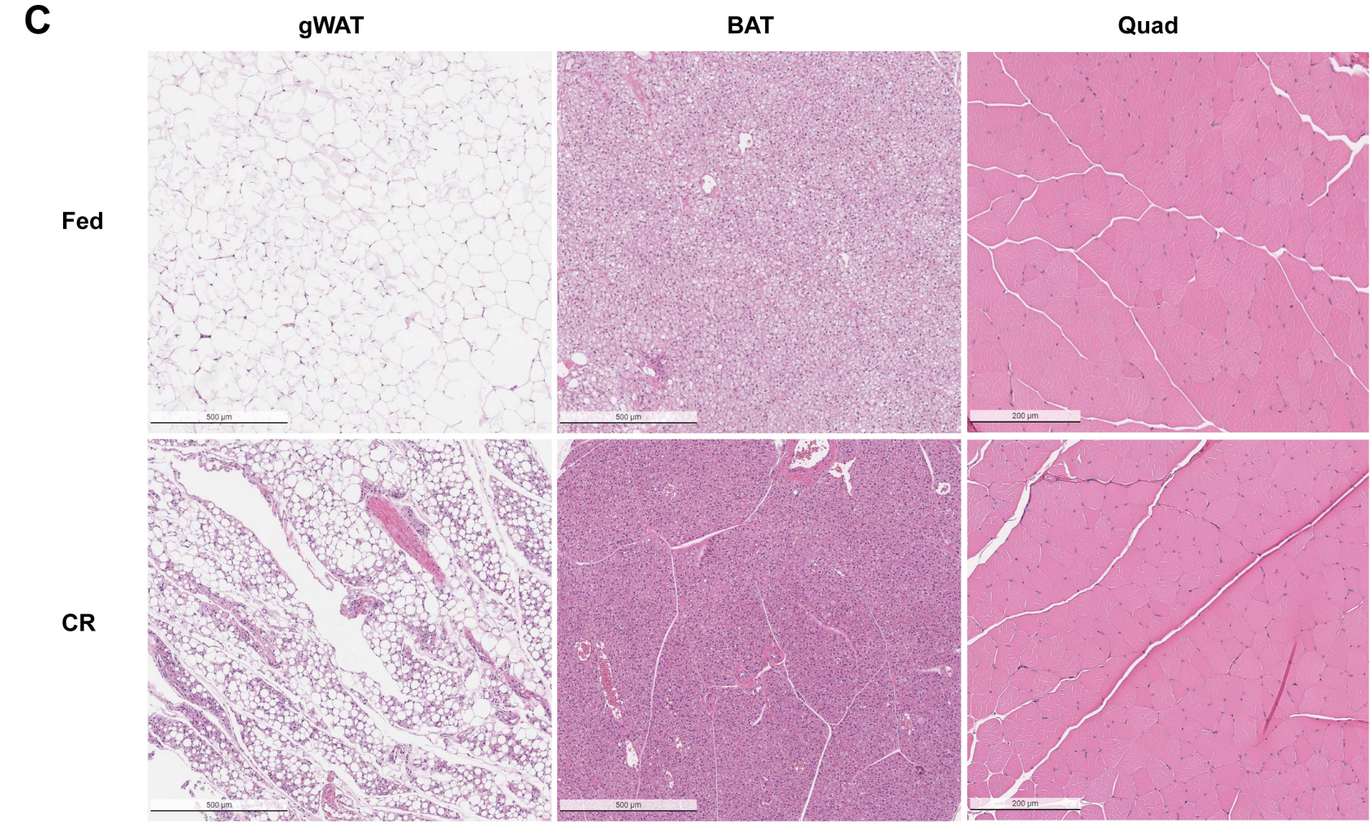
C
gWAT
BAT
Quad
Fed
CR
500 µm
500 µm
200 µm
500 µm
500 µm
200 µm

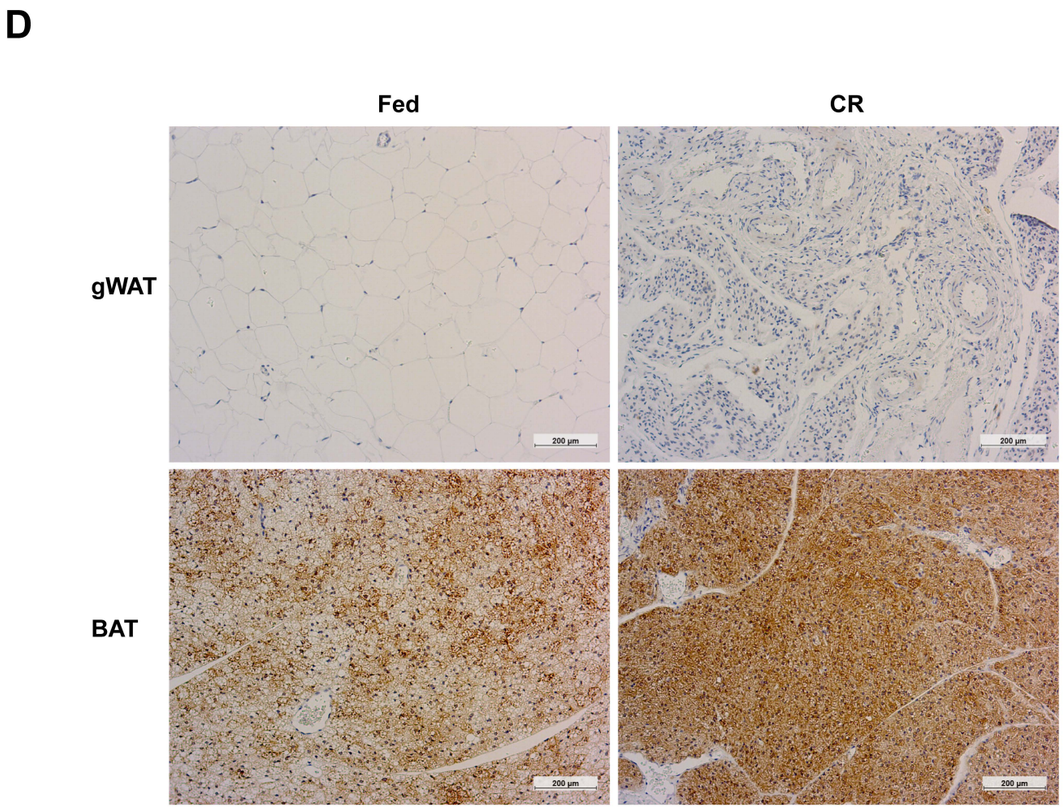
D
Fed
CR
gWAT
BAT
200 µm
200 µm
200 µm
200 µm

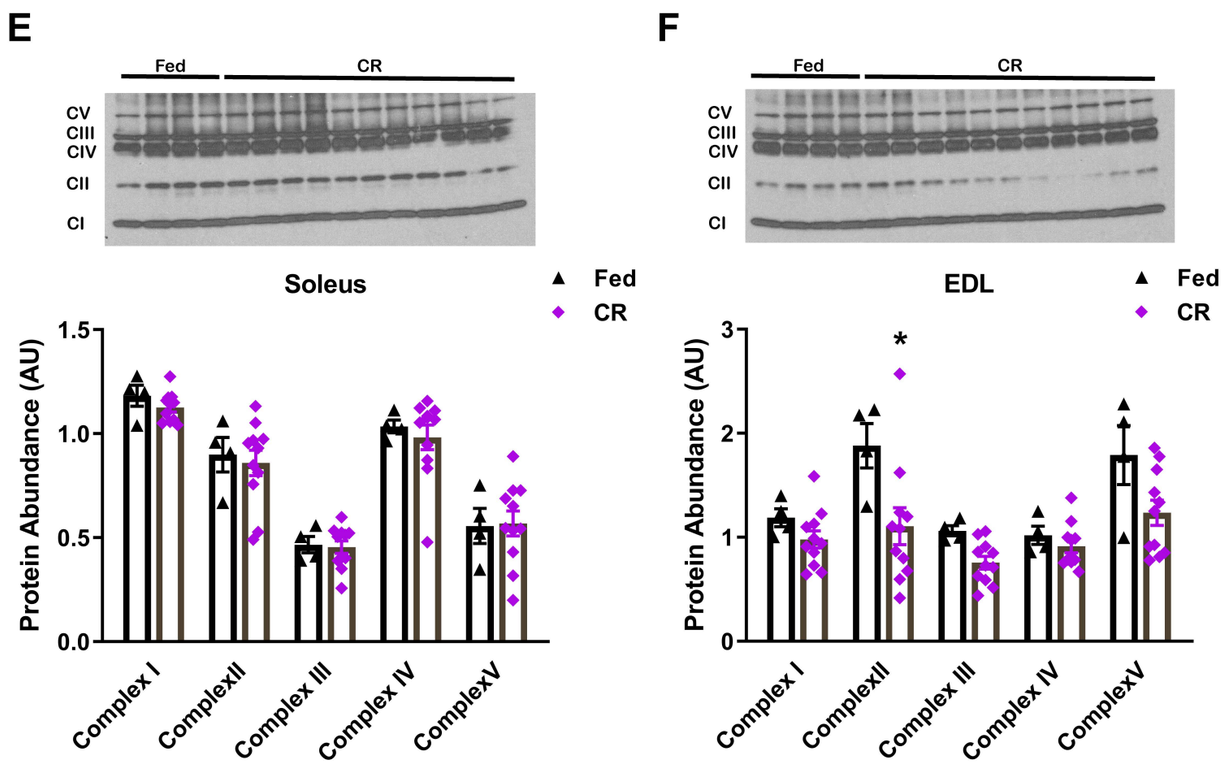
E
Fed
CR
CV
CIII
CIV
CII
CI
Soleus
Fed
CR
Protein Abundance (AU)
1.5
1.0
0.5
0.0
Complex I
ComplexII
Complex III
Complex IV
ComplexV
F
Fed
CR
CV
CIII
CIV
CII
CI
EDL
Fed
CR
*
Protein Abundance (AU)
3
2
1
0
Complex I
ComplexII
Complex III
Complex IV
ComplexV

Figure S8

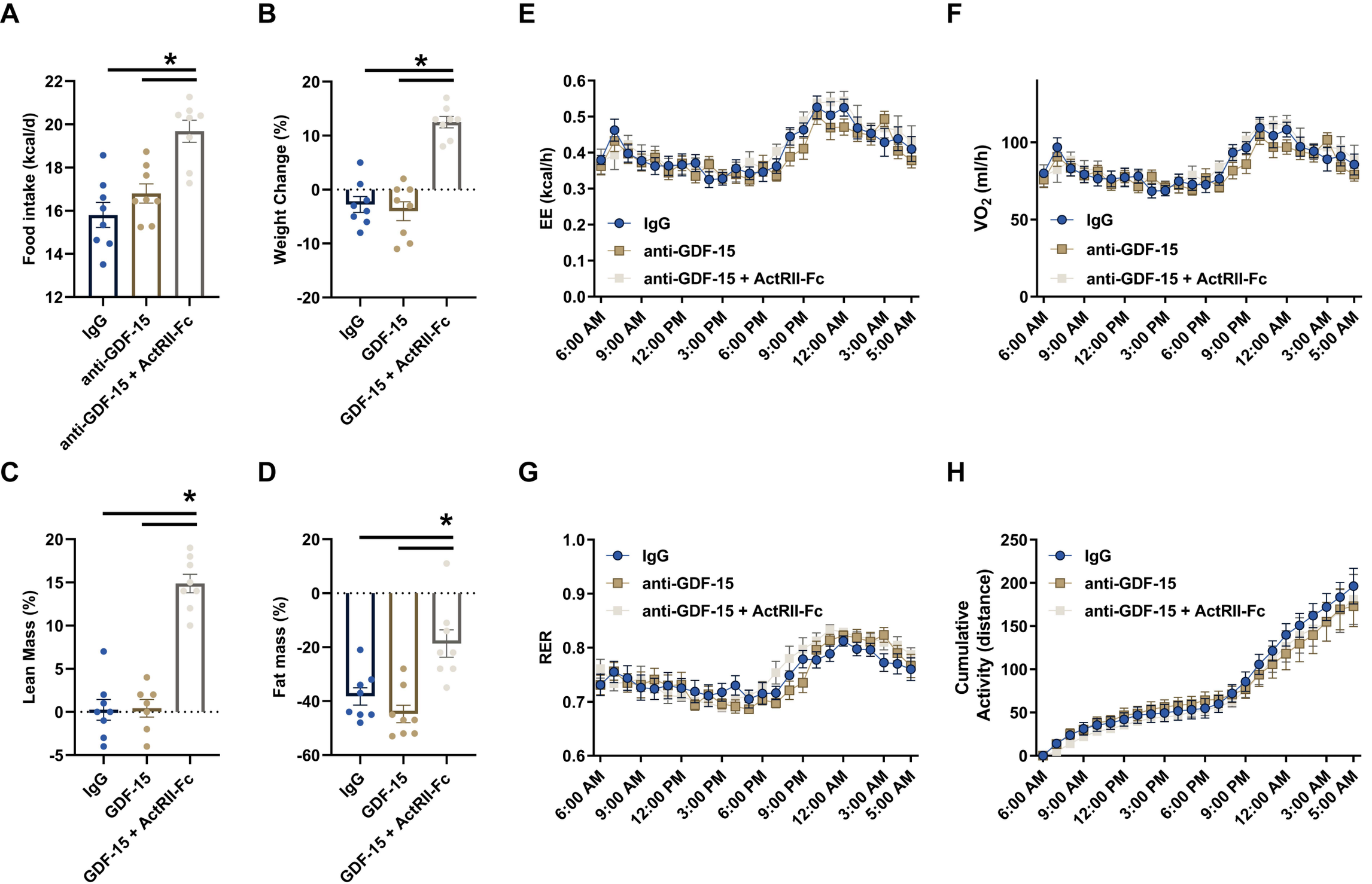
A
B
C
D
E
F
G
H
Food intake (kcal/d)
Weight Change (%)
Lean Mass (%)
Fat mass (%)
EE (kcal/h)
VO2 (ml/h)
RER
Cumulative Activity (distance)
IgG
anti-GDF-15
anti-GDF-15 + ActRII-Fc
GDF-15
GDF-15 + ActRII-Fc
6:00 AM
9:00 AM
12:00 PM
3:00 PM
6:00 PM
9:00 PM
12:00 AM
3:00 AM
5:00 AM
*

Figure S9

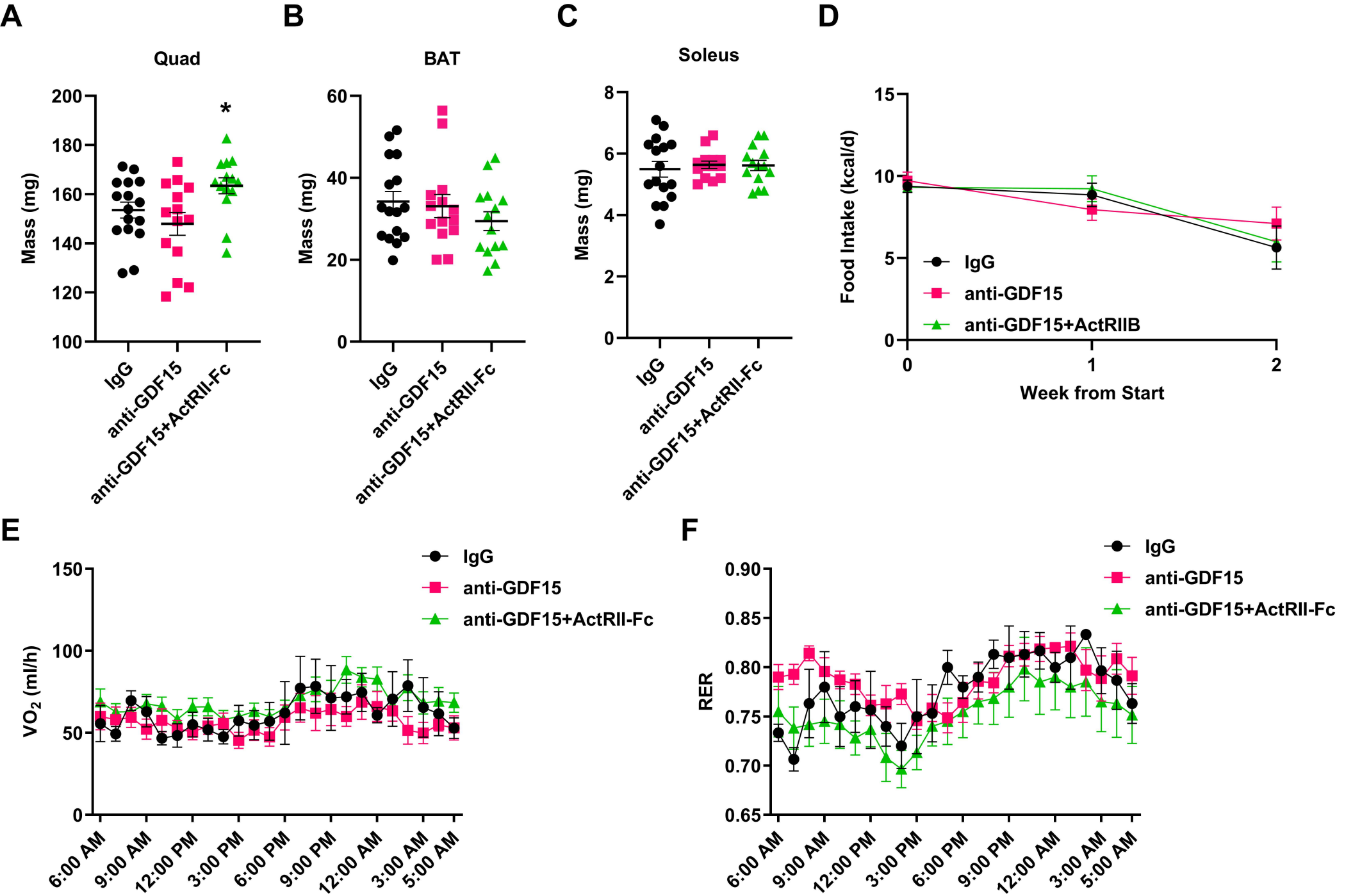
A
Quad
Mass (mg)
200
180
160
140
120
100
*
IgG
anti-GDF15
anti-GDF15+ActRII-Fc
B
BAT
Mass (mg)
60
40
20
0
IgG
anti-GDF15
anti-GDF15+ActRII-Fc
C
Soleus
Mass (mg)
8
6
4
2
0
IgG
anti-GDF15
anti-GDF15+ActRII-Fc
D
Food Intake (kcal/d)
15
10
5
0
0
1
2
Week from Start
IgG
anti-GDF15
anti-GDF15+ActRIIB
E
VO2 (ml/h)
150
100
50
0
6:00 AM
9:00 AM
12:00 PM
3:00 PM
6:00 PM
9:00 PM
12:00 AM
3:00 AM
5:00 AM
IgG
anti-GDF15
anti-GDF15+ActRII-Fc
F
RER
0.90
0.85
0.80
0.75
0.70
0.65
6:00 AM
9:00 AM
12:00 PM
3:00 PM
6:00 PM
9:00 PM
12:00 AM
3:00 AM
5:00 AM
IgG
anti-GDF15
anti-GDF15+ActRII-Fc

Figure S10

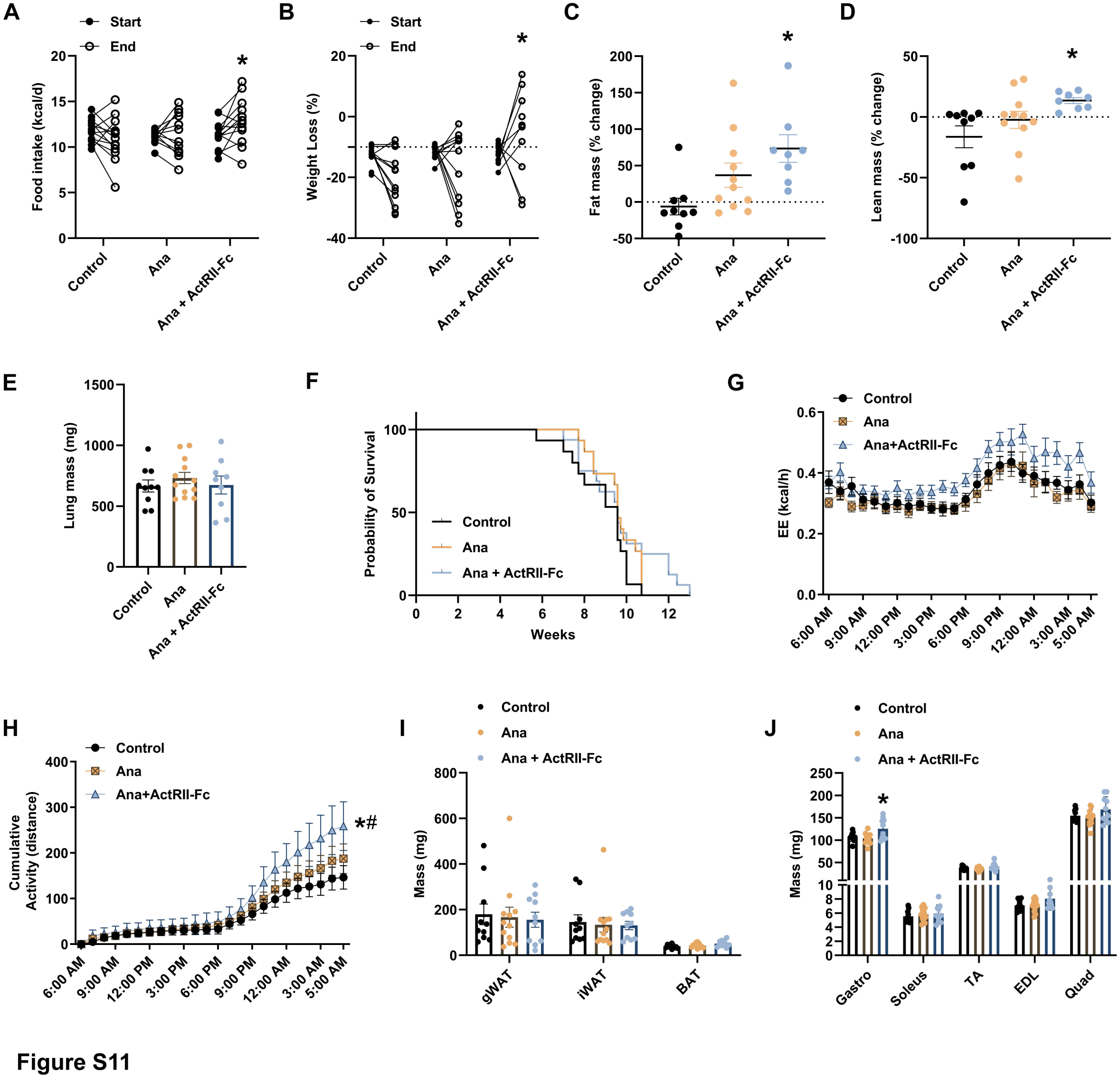
A
Start
End
Food intake (kcal/d)
Control
Ana
Ana + ActRII-Fc
B
Weight Loss (%)
C
Fat mass (% change)
D
Lean mass (% change)
E
Lung mass (mg)
F
Probability of Survival
Weeks
G
EE (kcal/h)
Control
Ana
Ana+ActRII-Fc
6:00 AM
9:00 AM
12:00 PM
3:00 PM
6:00 PM
9:00 PM
12:00 AM
3:00 AM
5:00 AM
H
Cumulative Activity (distance)
I
Mass (mg)
gWAT
iWAT
BAT
J
Gastro
Soleus
TA
EDL
Quad

Figure S11

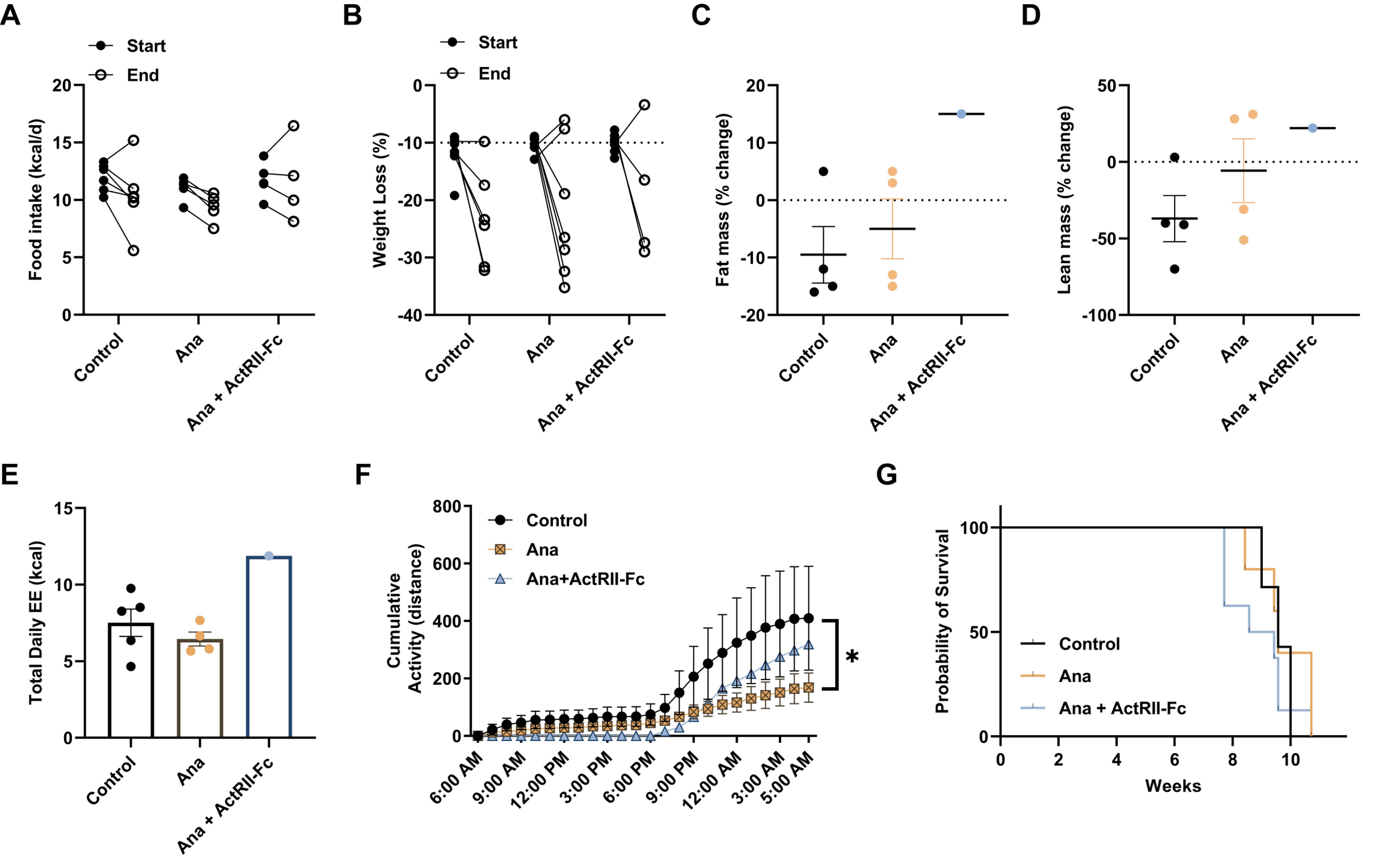
A
Start
End
Food intake (kcal/d)
20
15
10
5
0
Control
Ana
Ana + ActRII-Fc
B
Start
End
Weight Loss (%)
0
-10
-20
-30
-40
Control
Ana
Ana + ActRII-Fc
C
Fat mass (% change)
20
10
0
-10
-20
Control
Ana
Ana + ActRII-Fc
D
Lean mass (% change)
50
0
-50
-100
Control
Ana
Ana + ActRII-Fc
E
Total Daily EE (kcal)
15
10
5
0
Control
Ana
Ana + ActRII-Fc
F
Control
Ana
Ana+ActRII-Fc
Cumulative Activity (distance)
800
600
400
200
0
*
6:00 AM
9:00 AM
12:00 PM
3:00 PM
6:00 PM
9:00 PM
12:00 AM
3:00 AM
5:00 AM
G
Probability of Survival
100
50
0
Control
Ana
Ana + ActRII-Fc
0
2
4
6
8
10
Weeks

Figure S12